Doctor of Philosophy

ELECTRICALLY ASSISTED RAPID HEAT TREATMENTS IN SHEET METAL FORMING

The Graduate School of the University of Ulsan

School of Mechanical Engineering

Kieu-Anh Dinh

ELECTRICALLY ASSISTED RAPID HEAT TREATMENTS IN SHEET METAL FORMING

Advisor: **Sung-Tae Hong**

A Dissertation

Submitted to
the Graduate School of the University of Ulsan
In Partial Fulfillment of the Requirements
for the Degree of

Doctor of Philosophy

by

Kieu-Anh Dinh

School of Mechanical Engineering
Ulsan, Republic of Korea

Dec 2020

ELECTRICALLY ASSISTED RAPID HEAT TREATMENTS IN SHEET METAL FORMING

This certifies that the dissertation
of Kieu-Anh Dinh is approved

Committee Chair	Professor Doo-Man Chun
Committee Member	Professor Sung-Tae Hong
Committee Member	Professor Young-Jin Yum
Committee Member	Professor Koo-Hyun Chung
Committee Member	Dr. Moon-Jo Kim

School of Mechanical Engineering
Ulsan, Republic of Korea

December 2020

Kieu-Anh Dinh 의

공학박사 학위 논문을 인준함

심사위원	천두만	
심사위원	홍성태	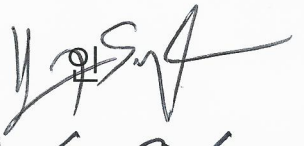
심사위원	염영진	
심사위원	정구현	
심사위원	김문조	

울산대학교 대학원

기계자동차공학과

2020 년 12 월

ELECTRICALLY ASSISTED RAPID HEAT TREATMENTS IN SHEET METAL FORMING

This certifies that the dissertation
of Kieu-Anh Dinh is approved

Committee Chair	Professor Doo-Man Chun
Committee Member	Professor Sung-Tae Hong
Committee Member	Professor Young-Jin Yum
Committee Member	Professor Koo-Hyun Chung
Committee Member	Dr. Moon-Jo Kim

School of Mechanical Engineering
Ulsan, Republic of Korea

December 2020

Kieu-Anh Dinh 의

공학박사 학위 논문을 인준함

심사위원	천두만	인
심사위원	홍성태	인
심사위원	염영진	인
심사위원	정구현	인
심사위원	김문조	인

울산대학교 대학원

기계자동차공학과

2020 년 12 월

Acknowledgment

First and foremost, I would like to express my sincerest gratitude to my supervisor, Professor Sung-Tae Hong, for his guidance and support which help me to complete this work. By his knowledge and greatly patience, he has given me many advices to help me throughout both my Ph.D. course and my thesis.

I would also like to thank Prof. Heung Nam Han and Dr. Moon-Jo Kim. They have kindly provided me with their specialist knowledge in the electroplasticity field.

I sincerely thank all my lab-mates at University of Ulsan and all Vietnamese friends for their friendship, enthusiastic help, and cheerfulness during my stay in Republic of Korea.

Finally, and the most important, I would like to thank my family for their support and encouragement during the period of my study. Especially, thank to my husband Dr. Xuan-Toa Tran and my little baby Enola for their great cared and encouragement me in the most difficult times.

Executive summary

Electrically assisted (EA) rapid heat treatment is a promising alternative heat treatment method, in which the microstructure and mechanical properties of a metal alloy are modified by simply applying pulsed electric current for a short duration in sheet metal forming process. The effectiveness of EA rapid heat treatment can be explained by the combination of the athermal effect of electricity and the thermal effect of rapid resistance heating.

Even though the performance of EA rapid heat treatment in sheet metal forming process surpasses that of conventional heat treating, the mechanism of electrical effect is not clearly identified yet. Also, the quantitative effect of electric current on the microstructure and resultant mechanical behavior has not been evaluated yet. The purpose of this study is to provide a precise processing technique in sheet metal forming (i.e., EA manufacturing), and to elucidate the post-EA rapid heating microstructure and mechanical behavior of the metal alloy during EA manufacturing process.

Firstly, a modified EA rapid heating of Al-Si coated hot stamping steel is suggested. The intermetallic evolution in the coating during heating is experimentally investigated. In the modified EA rapid heating, a continuous electric current for a suitable duration is applied to a specimen to heat it to a temperature slightly below the melting temperature of the coating. The temperature of the

specimen is then kept constant for specified dwell time. The result of the microstructural analysis shows that the modified EA rapid heating could effectively increase the thickness of the intermetallic layer between the coating and steel substrate much faster than conventional furnace heating and induction heating. The effectiveness of EA rapid heating may be due to the athermal effect of the electric current on the mobility of atoms, in addition to the well-known resistance heating effect. EA rapid heating also provides a technical advantage in that partial austenization can be easily achieved by properly placing the electrodes, as demonstrated in the present study.

Secondly, through the understanding of the mechanism of electricity effect during EA rapid heating, the effect of EA annealing on the mechanical behaviors of pre-strained two different aluminum alloys during EA dual-stage forming are experimentally investigated. First, a specimen is deformed to a specific pre-strain by uniaxial tension and then automatically unloaded. After that, the pre-strained specimen is subjected to EA annealing by electric current with a fixed subsecond duration. Finally, the specimen is reloaded until fracture. Experimental results show that application of electric current with a subsecond duration induces EA annealing to both pre-strained aluminum alloys. The electric current also increases total achievable elongation until fracture during EA dual-stage forming for both aluminum alloys. However, analysis of the stress-strain behavior during reloading and microstructural observations suggests that the quantitative effects of electric

current on the post-EA annealing mechanical behavior and resultant microstructure are strongly dependent on the type of aluminum alloy. Together, our findings indicate that while EA annealing is effective at improving the productivity of dual stage forming of an aluminum alloy, the composition of the aluminum alloy should be carefully considered in the design of the forming process utilizing the concept of EA annealing.

From this study, the concept of EA rapid heat treatment in sheet metal forming is suggested. Also, the intermetallic evolution of Al-Si coated hot stamping steel, and the mechanical behavior of pre-strained two different aluminum alloys during EA rapid heating are investigated clearly. The optimal condition to achieve the efficiency of the process is suggested considering both microstructure and mechanical behavior aspects. Through the athermal effect of electric current on the mobility of atoms, in addition to the well-known resistance heating effect, EA rapid heating is a feasible technique to apply in the real industry with the significant benefits in cycle time reduction.

Keywords: Electrically assisted rapid heat treatment, electrically assisted rapid heating, hot stamping, electrically assisted annealing, electrically assisted post welding heat treatment, partial austenization, pre-strain, dual stage forming, laser welding, Al-Si coated hot stamping steel, aluminum alloy, 590DP steel, uniaxial tensile test, flow stress, elongation, Vickers hardness, scanning electron microscope (SEM), electron backscatter diffraction (EBSD), X-ray diffraction (XRD), full width half maximum (FWHM), diffusion, intermetallic evolution, dislocation, annealing, recovery, recrystallization, precipitation, solid solution, joule heating, martensitic transformation, microstructure resetting, formability.

Student ID: 2014-5455

Contents

Chapter 1

Introduction

Chapter 2

Intermetallic evolution of Al-Si coated hot stamping steel during modified electrically assisted rapid heating

Chapter 3

The effect of pre-strain and subsequent electrically-assisted annealing on the mechanical behaviors of two different aluminum alloys

Chapter 4

Conclusion

List of tables

List of figures

Figure 3.14 The inverse pole figure maps of EA annealed 6061-T6 aluminum alloys: (a) 65%ε_{UTS} and (b) 85%ε_{UTS} pre-strain

Chapter 1

Introduction

1.1 Sheet metal forming

Sheet metal forming is among the basics of metalworking processes, where a sheet blank is plastically deformed into a complex three-dimensional geometry between tools to obtain the desired final configuration. Sheet metal forming operations are classified into two main processes. One is cold sheet metal forming, where the process is performed at lower than the recrystallization temperature. The other is warm or hot sheet metal forming, where the process is operated at elevated temperatures, such as hot stamping of boron steel or warm forming of aluminum alloy. In general, sheet metal forming also is classified according to the geometry of the formed part as clearly summarized in Table 1.1

Following are some general characteristics of sheet metal forming:

- The workpiece with a high ratio of surface area to thickness is entirely or partially subjected to plastic deformation.
- The plastic deformation is most commonly large and is the main factor to cause significant changes in shape. The sheet thickness reduction is not desirable since it can lead to necking and failure.
- Little or no material is removed during the forming process.

- Cold sheet metal forming may lead to increased mechanical properties, such as yield strength and tensile strength, due to the plastic strain accumulation.

Since the final part geometry could simply be produced in a very short time with scrap diminishing, sheet metal forming is a potential process to save both energy and material in manufacturing. However, the attempt to improve the efficiency of sheet metal forming process still attracts attention in both academia and industry.

Table 1.1 Commonly used sheet forming processes

Bending and straight flanging processes		
Brake bending	Hemming	Roll forming
Roll bending	Tube bending	Flanging
Hole flanging	Joggling	
Blank preparation		
Sheet leveling and straightening	Shearing, blanking, and piercing	
Deep drawing		
Deep drawing (using hard dies)	Sheet hydroforming with punch	Sheet hydroforming with die
Fluid bladder (diaphragm) forming	Malformed process	Drop hammer forming
Hot stamping		
Stretch forming		
Stretch forming asymmetric parts	Linear stretch forming	Creep forming
Age forming	Die quench forming	Bulging
Tube hydroforming	Expanding	Dimpling
Electromagnetic forming	Explosive forming	
Incremental forming		
Spinning	Shear forming	
Hybrid forming processes		
Ironing	Coining	Noising

1.2 Electroplasticity review

In the 1960s, the change of the dislocation movement in a superconductor during the transition between the superconducting stage and the normal stage had been extensively investigated. According to Tittmann and Bommel, the dislocation contribution to the ultrasonic absorption of superconducting lead was significantly less in the normal state than in the superconducting state [1,2]. Subsequently, many research studies have shown the similar phenomena occur to other mechanical properties, which influenced by the interaction of the dislocations and the conduction electrons, such as stress relaxation [3], flow stress change [4,5]. Even though the interaction between dislocation and electrons in metals was demonstrated, the exact underlying mechanism of this interaction remains controversial.

In 1969, Troistkii reported that the interaction between dislocations and electrons also exhibited when applying a high electric current pulse during the plastic deformation of metal [6]. Investigated on the flow stress reduction of zinc, cadmium, tin, lead, and indium during the pulsed current application, Troistkii suggested the term “electroplasticity” for the first time to imply the effect of electric current on the mechanical properties during deformation. However, the selected materials in Troistkii’s works somehow are still classified in the group of superconducting elements. Thenceforward, many scholars have studied to

demonstrate the effect of electric current on various metal alloys. Xu et al. suggested that the nucleation rate of strain-free grains during the recrystallization of cold-worked α-Ti could be promoted by electric current [7]. Chen et al. applied 5 A/mm^2 of pulsed electric current to Sn/Ag reaction couples and found that the electric current could either enhance or retard the growth of intermetallic compounds depending on the flow direction of electrons [8]. The investigations indicated that the electroplasticity is not limited to the superconducting elements.

At the early stages, the electroplasticity was investigated by applying continuous electric current to various metal alloys. In 2007, Andrawes et al. reported that applying electric current continuously would significantly reduce the energy needed to deform 6061-T6511 aluminum alloy without considerable heating the workpiece [9]. Also, the flow stress reduction of various metals (titanium-based alloys, iron, copper, and aluminum) influenced by a continuously applied electric current was evidenced in the work of Perkins et al. [10]. Although applying continuous electric current during metals' forming shows a great benefit in deformation force reduction, the achievable elongation decreases which leading to earlier fracture is an unavoidable impediment as clearly demonstrated by Ross et al. [11].

To address the limited formability of metals under a continuous electric current, applying high current density electropulsing during deformation has been

considered. In 2008, Roth et al. applied a pulsed electric current during the deformation of 5754 aluminum alloy and achieved elongation increases of nearly 400% of the gauge length [12]. Following this, Salandro et al. established the effect of electric current on aluminum alloys by examining the displacement of selected material during the tensile test [13]. The authors also proposed pulsing parameter sets which could be utilized to achieve the intended elongation during the tensile test of AZ31B-O magnesium alloy [14].

In order to understand the nature that accounts for the electroplasticity, many scholars have examined the effect of electric current on the mechanical behaviors of metals based on the microstructure aspect. Heigel et al. studied the microstructural alterations of 6061-T6511 aluminum alloy caused by applying pulsed current during deformation and found that both the number and size of precipitates are significantly affected [15]. The relationship between microstructure properties and the effect of electric current on C101 pure copper during the micro-extrusion test was examined by Siopis et al. [16,17]. It was concluded that the flow stress reduction influenced by pulsed current increases with increasing prior cold work and decreasing the grain size of the as-received specimen. Recently, Kim et al. studied the full width at half maximum (FWHM) of aluminum alloys and indicated the occurrent of annealing when applying pulsed electric current due to the annihilation of dislocations [18,19]. The authors also reported that electric current itself plays a distinct role in accelerating the formation of early-stage

precipitates from a supersaturated stage. Overall, investigating the effect of electric current on metals under microstructural observation has proved that the athermal effect caused by an electric current is distinct from the thermal effect caused by resistant heating.

With a foundation of the athermal effect contributed in electroplasticity, some researches commenced evaluating the effect of electric current on the mechanical behavior of metals. Kronenberger et al. determined the effects of electron flow on the 6061-T6511 aluminum alloy by subtracting out the obtained effects of resistive heating from a suggested finite element analysis model [20]. Bunget et al. suggested the term electroplastic effect coefficient to identify the amount of electric current effects that directly aids in deformation [21]. Two methods as mechanical-based and thermal-based approach to establish the electroplastic effect coefficient also are proposed by the authors. For the flow stress under electric current of metals, Salandro et al. proposed a methodology and examples of empirical modeling fabricated for both constant current density and non-constant current density [22]. In a study by Roh et al. a mathematical expression to describe the global stress-strain behaviors of 5052-H32 aluminum alloys under a pulsed electric current is suggested [23]. The empirical model is constructed utilizing two electroplastic coefficients as material constant and the other accounts for the effects of electric current density and electric pulse period. Even though the exact path of the stress-drop at the applying electric current still not obviously described, the proposed

empirical model exhibited a well prediction for the upper boundary of the ratchet shape stress-strain curve.

In general, even though a completely satisfactory explanation for the underlying physics that account for the electroplasticity mechanism of metals has not been provided yet, the application utilizing the electroplasticity phenomena is great potential in both academic and industrial fields.

1.3 Electrically assisted manufacturing

Recently, the application of electric current in the conventional manufacturing process is widely investigated due to the positive eletroplasticity effects as clearly indicated in chapter 1.2. The manufacturing process utilizing electroplasticity effects (i.e. electrically assisted manufacturing) is a promising alternative technique attempting to improve productivity, efficiency, and material properties [24,25]. A study on electrically assisted manufacturing (EAM) has been distributed into two main topics. One is electrically assisted forming, where electric current is applied to the workpiece during deformation [26]. The other is electrically assisted heat treatment, where the application of electric current is implemented without deformation [27]. For both topics, the principal benefits influenced by electric current include mechanical properties improvement and microstructure evolution.

In association with the increase of studies on electric current effects, the research into EAM process also rapidly expands. These processes include bulk deformation processes [28-30] and sheet metal forming processes [31,32] as summarized in figure 1.3.1. Additionally, EAM is considered to apply for other processes such as joining processes [33,34] and material-removal processes [35].

In comparison with conventional manufacturing process, the utilized EAM process exhibits various advantages. Since the electric current is basically generated by the power source, the required working place is much smaller and

simpler than that of conventional process equipped heating furnace as shown in figure 1.3.2. Also, conventional process requires excess time to heat up and maintain elevated temperatures of both the furnace and workpiece. Meanwhile, for EAM process, the temperature of the workpiece is rapidly heated to the intended temperature in a significantly shorter process time without heating the mold. Especially, the common drawbacks of conventional processes induced by elevated temperatures such as a wrap, surface oxidation could overcome in EAM due to the effectiveness of electric current at a relatively lower temperature. Therefore, EAM is a space-economizing and energy-saving manufacturing process while effectiveness enhancing the product quality.

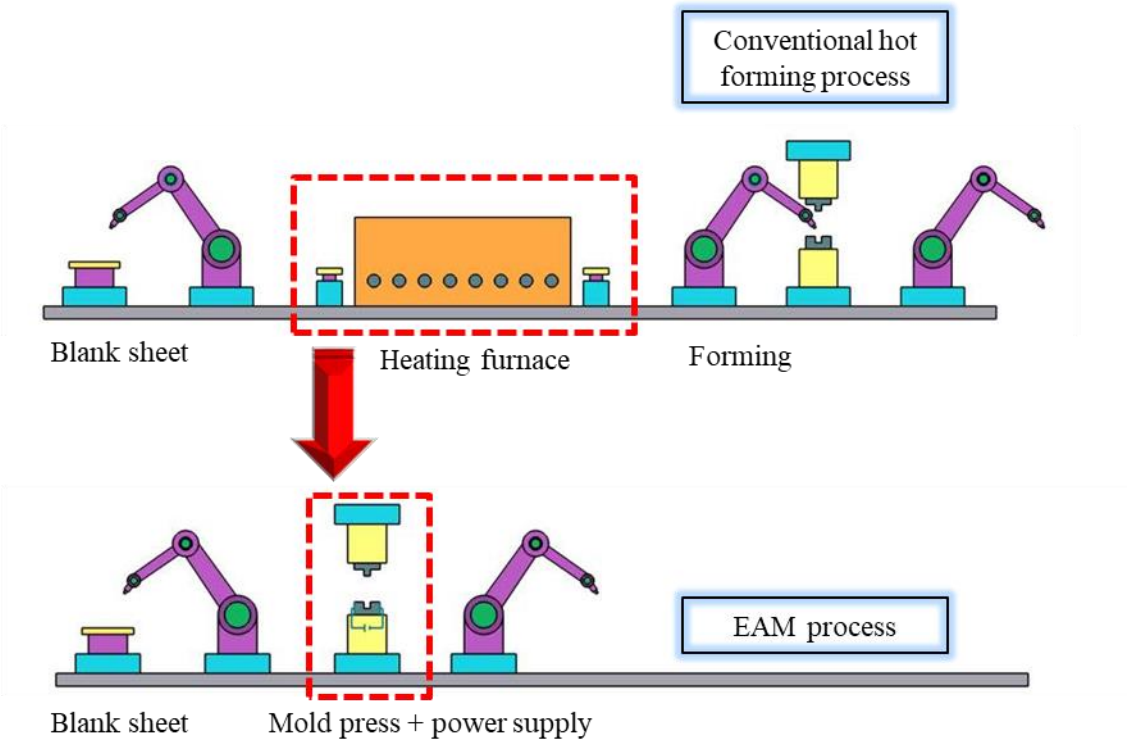

Figure 1.1 Conventional hot forming process and electrically assisted manufacturing process

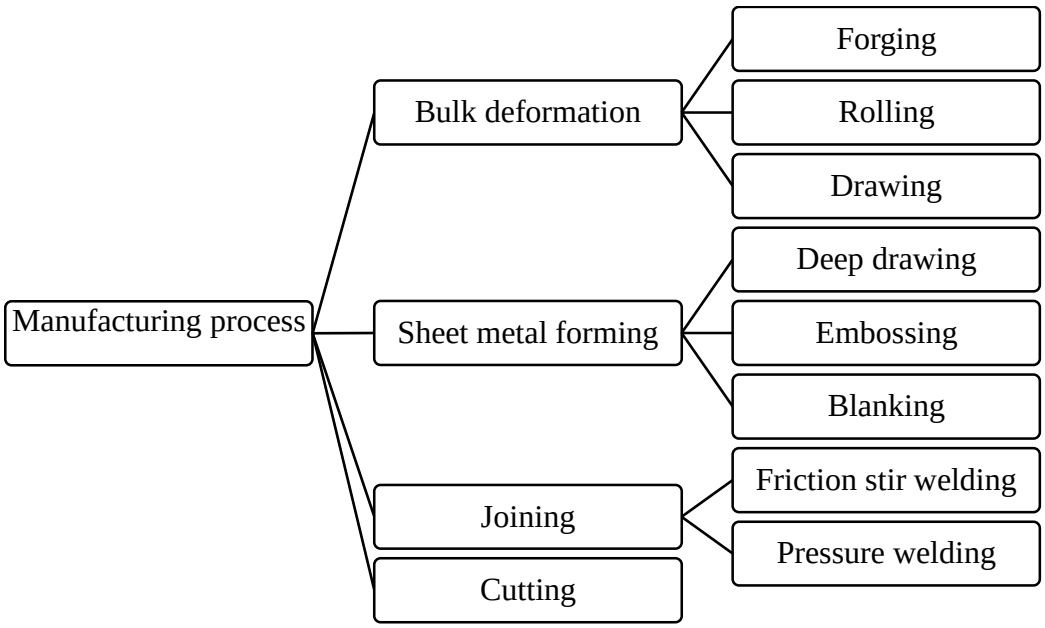

Figure 1.2 A list of electrically assisted manufacturing processes

1.4 Thesis motivation

Various scholars have been argued for the effectiveness of electroplasticity on metals recently. Electrically assisted manufacturing is a potential concept for conventional manufacturing processes based on the effects of electric current on metals. However, the application of EAM in the real industry process still exists impediment due to the lack of a clear understanding of electroplasticity mechanism. Also, the quantification of electroplasticity on the microstructure and resultant mechanical behavior is not evaluated yet. The purpose of this study is to provide a precise processing technique in sheet metal forming and to elucidate the post-EA rapid heating microstructure and mechanical behavior of the metal alloy during EAM process.

1.5 References for chapter 1

[1] Tittmann BR, Bömmel HE. Amplitude-Dependent Ultrasonic Attenuation in Superconducting Lead. Physical Review Letters. 1965 Mar 1;14(9):296.

[2] Tittmann BR, Bömmel HE. Amplitude-dependent ultrasonic attenuation in superconductors. Physical Review. 1966 Nov 4;151(1):178.

[3] Buck O, Alers GA, Tittmann BR. The effect of impurities on the flow stress change at the superconducting-normal transition. Scripta Metallurgica. 1970 Jul 1;4(7):503-7.

[4] Kojima H, Suzuki T. Electron drag and flow stress in niobium and lead at 4.2 K. Physical Review Letters. 1968 Sep 23;21(13):896.

[5] Alers GA, Buck O, Tittmann BR. Measurements of plastic flow in superconductors and the electron-dislocation interaction. Physical Review Letters. 1969 Aug 11;23(6):290.

[6] Troitskii O. Electromechanical effect in metals. ZhETF pisma redaktsiiu. 1969; 10:18.

[7] Xu ZS, Chen YX. Effect of electric current on the recrystallization behavior of cold worked α-Ti. Scripta Metallurgica. 1988 Jan 1;22(2):187-90.

[8] Chen CM, Chen SW. Electric current effects on Sn/Ag interfacial reactions. Journal of electronic materials. 1999 Jul 1;28(7):902-6.

[9] Andrawes JS, Kronenberger TJ, Perkins TA, Roth JT, Warley RL. Effects of DC current on the mechanical behavior of AlMg1SiCu. Materials and manufacturing processes. 2007 Jan 1;22(1):91-101.

[10] Perkins TA, Kronenberger TJ, Roth JT. Metallic forging using electrical flow as an alternative to warm/hot working.

[11] Ross CD, Irvin DB, Roth JT. Manufacturing aspects relating to the effects of direct current on the tensile properties of metals.

[12] Roth J, Loker I, Mauck D, Warner M, Golovashchenko S. Enhanced formability of 5754 aluminum sheet metal using electric pulsing. Transactions of the North America Manufacturing Research Institute of SME. 2008; 36:405-412.

[13] Salandro WA, Jones JJ, McNeal TA, Roth JT, Hong ST, Smith MT. Effect of electrical pulsing on various heat treatments of 5xxx series aluminum alloys. InASME 2008 International Manufacturing Science and Engineering Conference collocated with the 3rd JSME/ASME International Conference on Materials and Processing 2008 Jan 1 (pp. 283-292). American Society of Mechanical Engineers Digital Collection.

[14] Salandro W, Khalifa A, Roth J. Tensile formability enhancement of magnesium AZ31B-O alloy using electrical pulsing. Transations of the North American Manufacturing Research Institute of SME. 2009; 37:387-394.

[15] Heigel JC, Andrawes JS, Roth JT, Hoque ME, Ford RM. Viability of electrically treating 6061 T6511 aluminum for use in manufacturing processes.

[16] Siopis MS, Kinsey BL. Experimental investigation of grain and specimen size effects during electrical-assisted forming. Journal of manufacturing science and engineering. 2010 Apr 1;132(2).

[17] Siopis MS, Kinsey BL, Kota N, Ozdoganlar OB. Effect of severe prior deformation on electrical-assisted compression of copper specimens. Journal of manufacturing science and engineering. 2011 Dec 1;133(6).

[18] Kim MJ, Lee K, Oh KH, Choi IS, Yu HH, Hong ST, Han HN. Electric current-induced annealing during uniaxial tension of aluminum alloy. Scripta Materialia. 2014 Mar 15; 75:58-61.

[19] Kim MJ, Lee MG, Hariharan K, Hong ST, Choi IS, Kim D, Oh KH, Han HN. Electric current–assisted deformation behavior of Al-Mg-Si alloy under uniaxial tension. International Journal of Plasticity. 2017 Jul 1; 94:148-70.

[20] Kronenberger TJ, Johnson DH, Roth JT. Coupled multifield finite element analysis model of upsetting under an applied direct current. Journal of manufacturing science and engineering. 2009 Jun 1;131(3).

[21] Bunget C, Salandro WA, Mears L, Roth JT. Energy-based modeling of an electrically-assisted forming process. Transactions of the North American Manufacturing Research Institute of MSE. 2010;38.

[22] Salandro WA, Bunget C, Mear L. Modeling the electroplasticity effect during electrically assisted forming of 304 stainless steel. ASME international manufacturing science & engineering conference. 2012; 7241:10.

[23] Roh JH, Seo JJ, Hong S-T, Kim M-J, Han HN. The mechanical behavior of 5052-H32 aluminum alloys under a pulsed electric current. International Journal of Plasticity. 2014; 58:84-99.

[24] Chu WS, Kim CS, Lee HT, Choi JO, Park JI, Song JH, Jang KH, Ahn SH. Hybrid manufacturing in micro/nano scale: A Review. International journal of precision engineering and manufacturing-green technology. 2014 Jan 1;1(1):75-92.

[25] Nguyen-Tran HD, Oh HS, Hong ST, Han HN, Cao J, Ahn SH, Chun DM. A review of electrically-assisted manufacturing. International Journal of Precision Engineering and Manufacturing-Green Technology. 2015 Oct 1;2(4):365-76.

[26] Niebauer J, Grimm T, Shaffer D, Sweeney I, Ragai I, Roth JT. Effect of Applied Electricity on Springback During Bending and Flattening of 304/316 Stainless Steel, Titanium AMS-T-9046 and Magnesium AZ31B. InASME 2016

11th International Manufacturing Science and Engineering Conference 2016 Jan 1. American Society of Mechanical Engineers Digital Collection.

[27] Park GD, Hong ST, Jeong YH, Yeo TS, Nam MJ, Kim MJ, Jin SW, Han HN. Electrically assisted stress relief annealing of automotive springs. Journal of Mechanical Science and Technology. 2017 Aug 1;31(8):3943-8.

[28] Jones JJ, Mears L, Roth JT. Electrically-assisted forming of magnesium AZ31: Effect of current magnitude and deformation rate on forgeability. Journal of Manufacturing Science and Engineering. 2012 Jun 1;134(3).

[29] Ng MK, Fan Z, Gao RX, Smith III EF, Cao J. Characterization of electrically-assisted micro-rolling for surface texturing using embedded sensor. CIRP Annals. 2014 Jan 1;63(1):269-72.

[30] Tang G, Zhang J, Yan Y, Zhou H, Fang W. The engineering application of the electroplastic effect in the cold-drawing of stainless-steel wire. Journal of materials processing technology. 2003 Jun 30;137(1-3):96-9.

[31] Mai J, Peng L, Lai X, Lin Z. Electrical-assisted embossing process for fabrication of micro-channels on 316L stainless steel plate. Journal of Materials Processing Technology. 2013 Feb 1;213(2):314-21.

[32] Kim W, Yeom KH, Thien NT, Hong ST, Min BK, Oh SI, Kim MJ, Han HN, Lee HW. Electrically assisted blanking using the electroplasticity of ultra-high strength metal alloys. CIRP Annals. 2014 Jan 1;63(1):273-6.

[33] Potluri H, Jones JJ, Mears L. Comparison of electrically-assisted and conventional friction stir welding processes by feed force and torque. InASME 2013 International Manufacturing Science and Engineering Conference collocated with the 41st North American Manufacturing Research Conference 2013. American Society of Mechanical Engineers Digital Collection.

[34] Li YF, Hong ST, Choi H, Han HN. Solid-state dissimilar joining of stainless steel 316L and Inconel 718 alloys by electrically assisted pressure joining. Materials Characterization. 2019 Aug 1; 154:161-8.

[35] Baranov SA, Staschenko VI, Sukhov AV, Troitskiy OA, Tyapkin AV. Electroplastic metal cutting. Russian Electrical Engineering. 2011 Sep 1;82(9):477-9.

Chapter 2

Intermetallic evolution of Al-Si coated hot stamping steel during modified electrically assisted rapid heating

2.1 Introduction

In the automotive industry, due to the pressing demands of not only safety performance but also respect for the environment, the use of ultra-high-strength steel (UHSS) for lightweight automotive structures is a frequently considered strategy. UHSS is known to provide mechanical characteristics, including high-strength-to-density ratio and improved toughness, which satisfy the requirements of body-in-white component manufacturing such as B-pillar reinforcements, inner roof rails, and longitudinal rear rails.

However, applying UHSS to traditional sheet forming technologies induces various well-known technical difficulties. As the strength of the steel sheet increases, the essential forming load increases, and thus, the springback becomes larger [1–3]. The deformed parts can lack precision and contribute to structural defects such as cracks, wrinkles, and rough surfaces. Moreover, a high forming load during forming may cause deterioration of the forming equipment.

In order to overcome these drawbacks, hot stamping has been effectively used as a forming technology for UHSS. Hot stamping is a non-isothermal process carried out at high temperatures with the intention of eliminating springback [4]. Boron steel (typically 22MnB5) is commonly used as a material in the hot stamping process. Many researchers have carried out studies to investigate the thermomechanical flow properties of hot stamping steel during the hot stamping process. Merklein and co-researchers demonstrated that the forming ability of the hot stamping steel depends on the temperature, strain rate, and cooling rate [5,6]. In the hot stamping process, a boron steel sheet is heated slightly above the $\gamma \rightarrow \alpha$ transition temperature for a relevant dwell time to allow homogeneous austenization. Then, the heated sheet with a reduced flow stress (about 200 MPa) is deformed and subsequently die-quenched to achieve a tensile strength of about 1350 MPa [7–9]. It is well known that the rapid cooling rate during die quenching creates a microstructure with a refined martensitic phase arrangement and uniformly distributed hardness without cracking [10].

The heating process is extremely important in hot stamping. Commonly employed methods are conventional heating using roller hearth furnaces [11] or induction heating using eddy currents [12,13]. Electrically assisted (EA) rapid heating (known as a smart hot stamping process), which was suggested by Mori et al. [14] can be an alternative heat treatment method in which the temperature is rapidly increased by resistance heating. This method can also induce partial heating

in which a specific area of the specimen can be selectively heated. Therefore, EA rapid heating allows for forming inhomogeneous characteristic components such as the automotive B-pillar. For the automotive B-pillar, it is beneficial if the upper part has a martensitic structure to resist intrusion crashes, whereas the bottom part has a mixed bainitic and martensitic structure to absorb the crash impact. In hot stamping, as a result of the elevated temperature, oxidation and decarburization on the surface of the heated steel sheet are generally inevitable. To prevent the aforementioned negative phenomena and to improve the corrosion resistance, a thin aluminized coating covering the surface of the boron steel substrate is frequently used [15]. There are two major types of hot-dip aluminized coatings currently used for hot stamping sheets. The first type consists of an Al–Si alloy (7–11 wt% Si) which provides considerable coating resistance to oxidation and corrosion at elevated temperatures. The second type is pure aluminum with high reflection, which is mainly applied for reflective surface purposes [10]. Therefore, the first type (Al–Si coating) is extensively used to manufacture automotive hot stamping components and is the main subject of the present study.

During the hot stamping process, the transformation of the Al–Si coating to an Al–Si–Fe intermetallic layer is imperative. The intermetallic layer, which is thermodynamically stable at temperatures higher than the melting temperature of the original Al–Si alloy, will protect the steel substrate from inner penetrating oxidation and surmount the thermal expansion coefficient mismatch between the

coating and steel substrate. In conventional methods, the intermetallic evolution could be naturally achieved via the slow heating rate. Borsetto et al. [16] showed that the steel diffusion process from the coating–substrate interface to the coating layer is thermally activated during hot stamping. Gui et al. [17] reported transformation of the Al– Si coating into Fe–Al intermetallic compounds after austenizing at 920 °C for 5 min. It was also shown that the coating was composed of multiple intermetallic layers and a diffusion layer after heat treatment [18]. However, in the case of EA rapid heating, the development of intermetallic phases can be more difficult. Due to the rapid heating rate, the melting phenomenon dominates prior to a sufficient degree of intermetallic evolution in the Al–Si coating. In the present study, a solution to this technical difficulty is described (the modified EA rapid heating) and the corresponding intermetallic evolution of the Al–Si coating during the heating process is experimentally investigated.

2.2 Experimental procedures

Commercially available 22MnB5 boron steel sheets (thickness of 1.1 mm) with hot-dipped coating layers (20 μm Al-10 wt% Si) on the top and the bottom surfaces were used. The chemical composition of the primary steel substrate sheet is listed in Table 2.1. The presence of Mn and B elements in the chemical composition is beneficial to increase the hardenability and retard the heterogeneous nucleation of

ferrite at the austenite grain boundaries. Specimens with a size of 250 mm × 80 mm were prepared from the boron steel sheet along the rolling direction.

Table 2.1 Chemical compositions (in wt.%) of the hot stamping steel sheet

C	Mn	Si	Al	Ti	B	Fe
0.20-0.25	1.10-1.30	0.15-0.35	0.02-0.06	0.02-0.05	0.002-0.004	At balance

The experimental setup for the modified EA rapid heating consists of a power supply, two connecting cable wires, flat copper electrodes, and the test specimen, as schematically described in Fig. 2.1. A Vadal SP-1000U welder (Hyosung, South Korea) was used to generate a pulsed electric current and was operated using a programmable pulse controller. The copper electrodes were used to homogeneously distribute the electric current flowing through the specimen from the cathode to the anode. In order to avoid electric sparks at the electrode-specimen interface, the specimen was cleaned using ethanol prior to the experiment and tightly clamped using a press clamp. A set of bakelite insulators was used to insulate the experimental setup and guarantee the safety of the entire system.

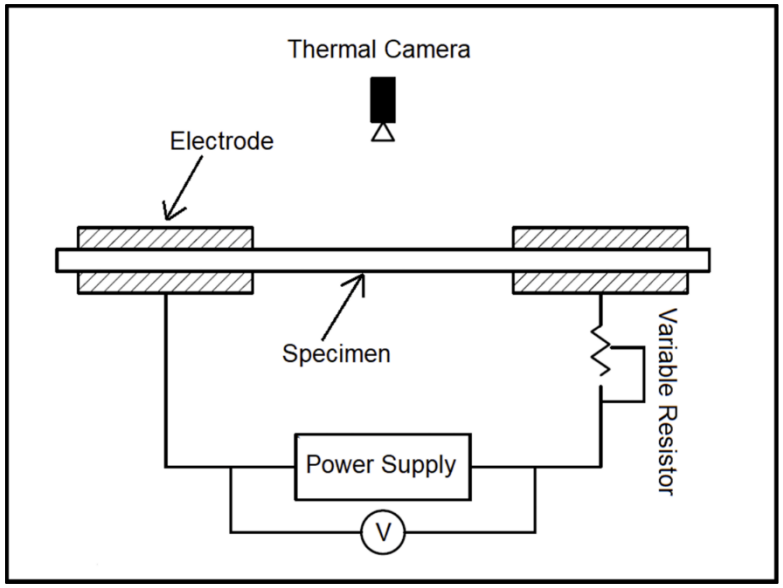

Figure 2.1 A schematic of the experimental set-up

The modified EA rapid heating of the Al–Si-coated hot stamping steel specimen is schematically described in Fig. 2.2. First, the specimen is rapidly heated to a temperature slightly lower than the melting temperature of the Al–Si coating (570 °C) by a continuous electric current. A pulsed electric current with a short duration is then applied to the specimen to keep the temperature isothermal for the specified dwell time. In the actual hot stamping process with modified EA rapid heating, the specimen would be heated by a continuous current again over the full austenization temperature after the isothermal dwell time, as described by the dashed line in Fig. 2.2. However, in the present study, the specimen was immediately water-quenched after the dwell time to observe the intermetallic evolution in the Al–Si coating during the dwell time by the pulsed electric current. The mechanical and microstructural properties of hot-stamped steels after full austenization followed by quenching have been discussed in many reports and will not be repeated here.

In the modified EA rapid heating experiment, the specimen was heated using the electric current parameters listed in Table 2.2, which were selected as a result of separately conducted preliminary studies. Three different dwell times, 0, 10, and 25 s, were considered in the modified EA rapid heating experiments. The temperature history along the surface of the specimen was monitored by an infrared thermal imaging camera (FLIR-T621, FLIR Systems, Oregon, USA) throughout the experiment. High-temperature black paint was applied to the surface of the

specimen to stabilize the emissivity. The thermal imaging camera was then calibrated based on preliminary tests using a K-type thermocouple.

To evaluate the effect of electric current on the intermetallic evolution in the Al–Si coating, comparative experiments were also carried out utilizing two conventional heating methods, furnace heating (FH) and induction heating (IH). In furnace heating, the specimen was placed in a resistant furnace (Nabertherm Labotherm N7/H/B150, Nabertherm GmbH, Germany) to reach the target temperature of 570 °C, and it was held at the target temperature for 25 s before water quenching. Note that the heating rate of the furnace heating was approximately 3 °C/s, which is significantly lower than that of modified EA rapid heating. Therefore, the specimen in the furnace heating was actually exposed to an elevated temperature for a significantly longer time than the specimen in the modified EA rapid heating. In the furnace heating test, a K-type thermocouple was physically attached to the surface of the specimen to monitor the temperature history. During induction heating, the temperature of the specimen was increased to the target temperature of 570 °C in 3 s and held constant over the 25 s dwell time. Once again, a K-type thermocouple was used to monitor the temperature history. It is well known that induction heating utilizes eddy currents, which is a skin (or surface) effect [19]. Therefore, the heating mechanism of induction heating is quite different than that of directly applying an electric current to the specimen. Thermal homogeneity during induction heating is mainly achieved by thermal conduction.

Table 2.2 Process parameter for modified electrically assisted rapid heating

Specimen	Continuous electric current		A pulsed electric current			
	Electric current density* (A/mm^2)	**Duration (sec)**	**Electric current density* (A/mm^2)**	**Duration (sec)**	**Period (sec)**	**Number of pulses**
EA-0	57	3	-	-	-	-
EA-10			14	2	2	3
EA-25						6

*Base on the original cross-sectional area of the specimen

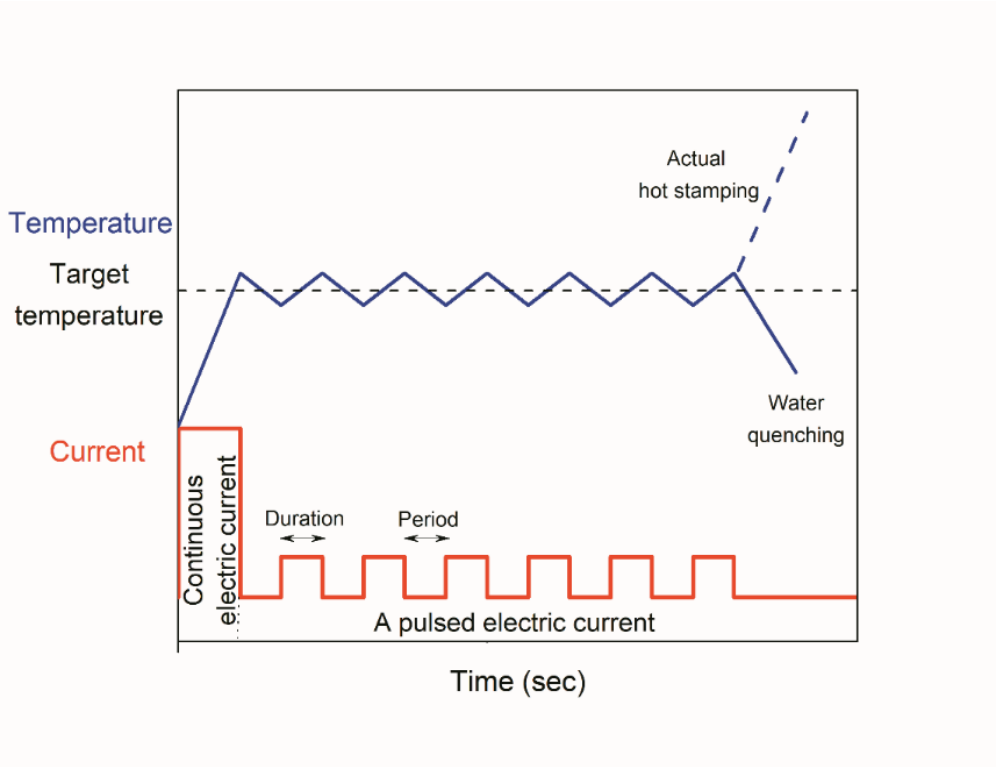

Figure 2.2 A schematic of the procedure of modified electrically assisted rapid heating

Microstructural analysis was performed via confocal laser scanning microscopy and a field emission gun scanning electron microscope (FE-SEM, Merlin compact, Carlzeiss, Germany) equipped with energy-dispersive X-ray spectroscopy (EDS). Samples for the microstructural analysis were obtained from the tested specimens using a low-cycling diamond saw with dimensions of 1 mm × 1 mm. Then, they were embedded in an electrically conductive polymer matrix. The cross sections of the samples were then prepared along the direction of the electric current by standard metallographic grinding and polishing finished with a 1-μm diamond suspension followed by electropolishing using 10% perchloric acid.

2.3 Results and Discussion

In modified EA rapid heating, the average temperature of the heated region of the specimen reached the target temperature in 3 s (average heating rate of 190 °C/s) and was held nearly constant for the given dwell time, as shown in the temperature history of the EA-25 specimen (Fig. 2.3a). The temperature profile long the length of the EA-25 specimen at 1 s after the initiation of the dwell period also confirms that the temperature of the heated region was nearly uniform along the length at the target temperature (Fig. 2.3b). As marked in Fig. 2.3b, the temperature profile along the length of the specimen clearly shows three different temperature regions, a high-temperature (heated) region, transition region, and unheated region. At the edges of the electrodes, temperature transition regions exist, and unheated regions are

observed underneath the electrodes. The temperature history and profile in Fig. 2.3 confirm that the dwell at the target temperature could be easily achieved by applying a properly designed pulsed electric current.

(a)

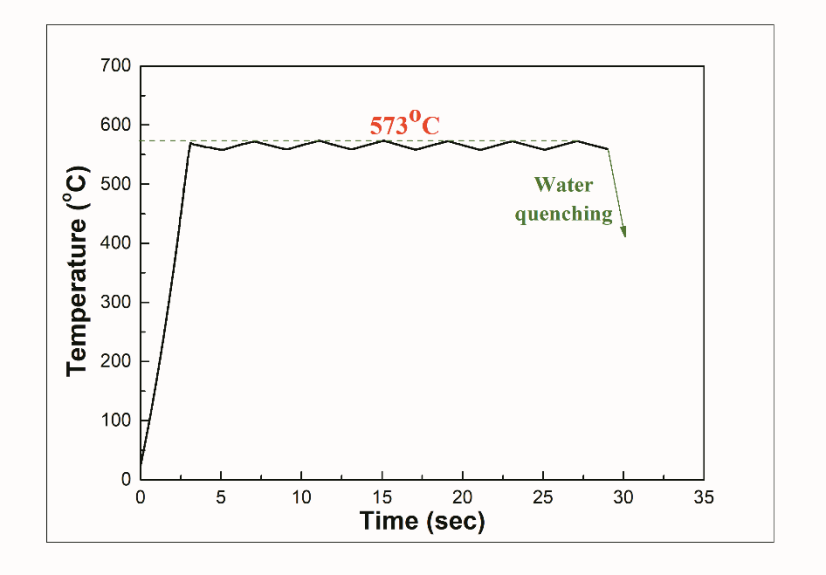

(b)

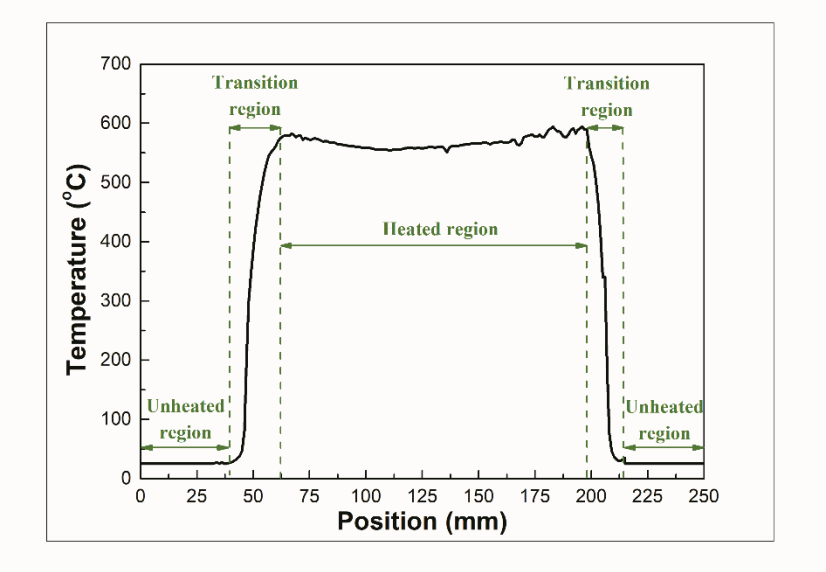

Figure 2.3 (a) Temperature history of EA-25 specimen, (b) temperature profile along the length of the EA-25 specimen at 1 s after the initiation of the dwell period

The results of the SEM-EDS analysis on the cross section of the heated region show that the intermetallic evolution was significantly accelerated by the electric current. The thickness of the Al-Si coating of the as-received specimen prior to heating experiment was measured to be 18.48 ± 1.6 μm. The cross-section of the as-received specimen consists of three separate zones as marked in Fig. 2.4. Zone I describe the Al-Si coating, which has silicon aggregates embedded in the aluminum matrix. Note that the silicon element in the coating composition contributes to diminish the coating thickness and to flatten the interface between the coating and the boron steel substrate during hot dip process [20-22]. Zone II is the a thin Fe_2SiAl_7 intermetallic layer between the coating and the steel substrate, which was induced from the earlier hot dip process. This zone is discontinuous along the length of the specimen with the maximum thickness close to 2.3 μm. Zone III is simply the boron steel substrate.

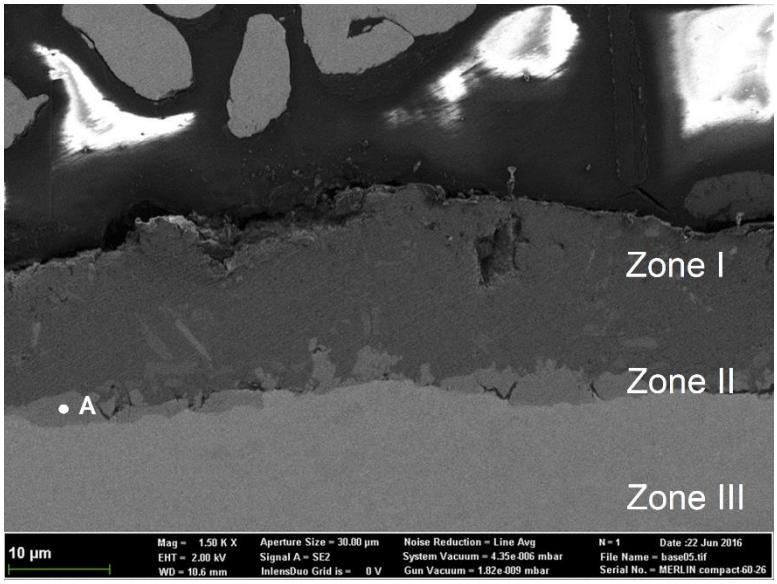

Figure 2.4 Cross-sectional SEM-EDS micrograph of as-received specimen

The cross-sectional microstructures of the coating after the heating experiments are shown in Fig. 2.5. Note that silicon has a similar atomic radius and molecular weight to aluminum. Therefore, it is assumed that silicon behaves similarly to aluminum in the coating for the microstructure analysis, and the coating is assumed to follow the binary Al–Fe diagram in the present study [23]. At the dwell temperature (570 °C), the intermetallic evolution in the coating depends on the diffusion between aluminum–silicon in the coating and boron steel substrate [24].

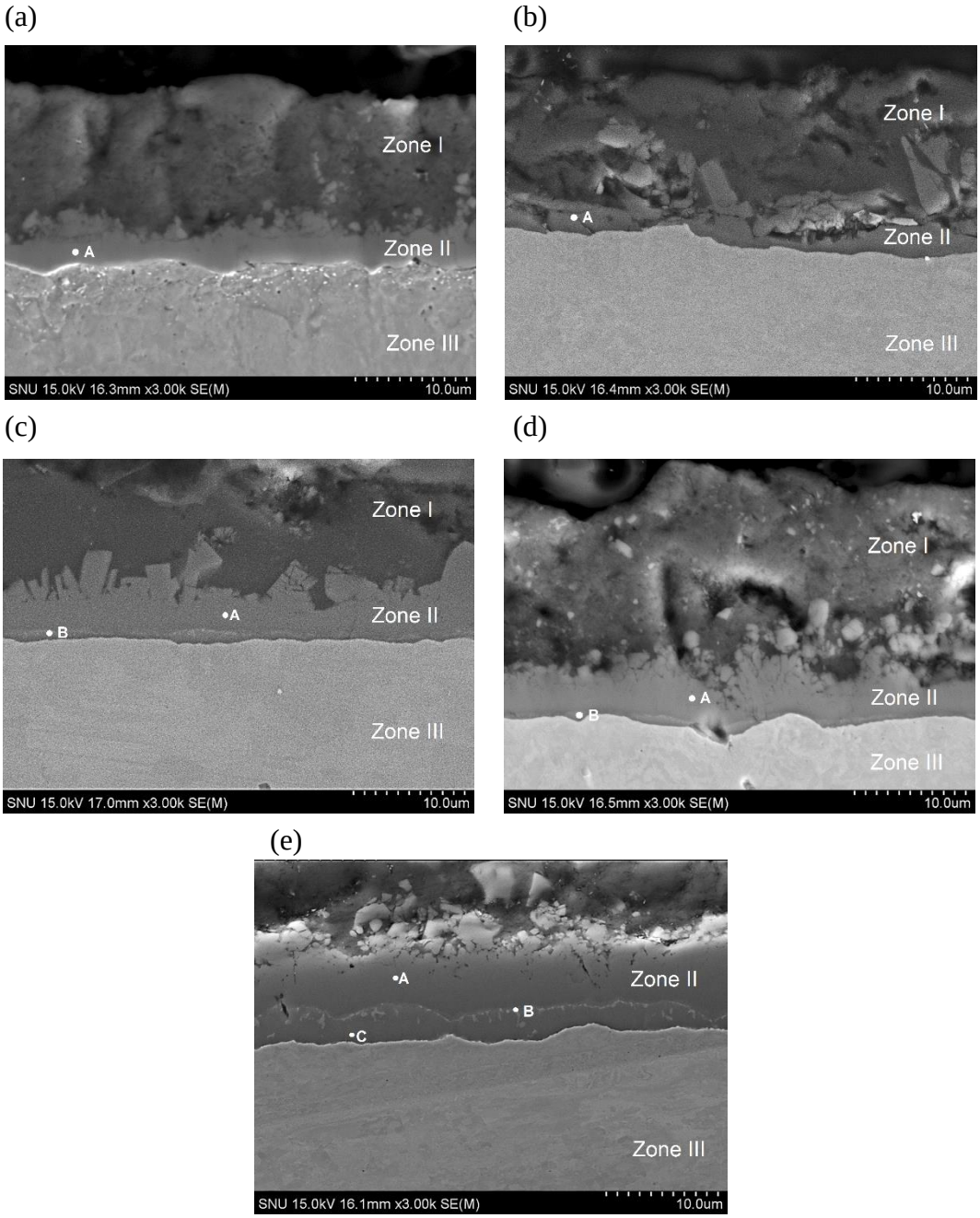

Figure 2.5 Cross-sectional SEM-EDS micrograph of (a) CH specimen, (b) IH specimen, (c) EA-0 specimen, (d) EA-10 specimen, (e) EA-25 specimen

As indicated in Fig. 2.5 and summarized in Fig. 2.6, compared to the as-received specimen, the thickness of the intermetallic layer (zone II) of the heat-treated specimens increased for all three of the heating methods. It is very interesting to note that the diffusion process between the coating and boron steel substrate was significantly enhanced in the modified EA rapid heating process compared to furnace or induction heating. Even with a dwell time of 0 s, the intermetallic layer of the specimen after the modified EA rapid heating (5.04 ± 0.66 μm) became thicker than the intermetallic layers of the specimens obtained after furnace heating (3.75 ± 0.13 μm) and induction heating (3.24 ± 0.58) with dwell times of 25 s. Note that the results of furnace heating and induction heating are quite similar. In contrast to furnace and induction heating, the intermetallic evolution of the coating was nearly completed in the modified EA rapid heating process (9.56 ± 0.8 μm) with a dwell time of 25 s. Note that a thin oxide layer (Al_2O_3) was observed at the outer surface of coating for all the heat-treated specimens, probably due to heating in air and quenching in water.

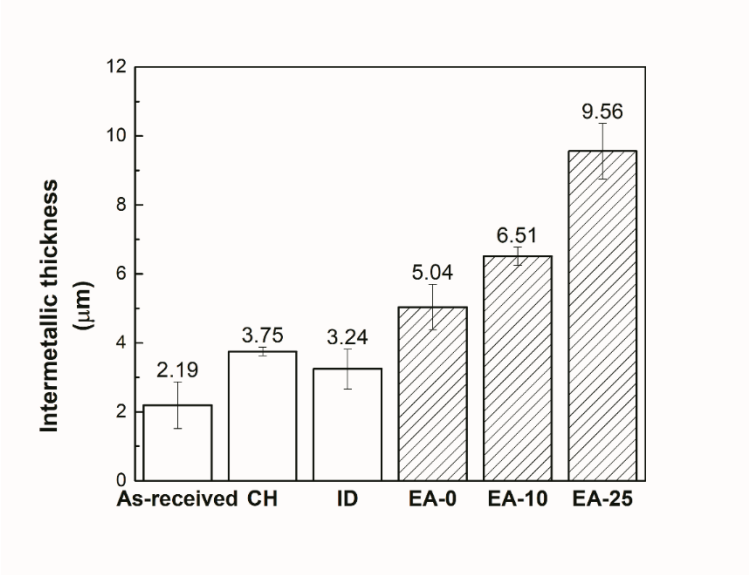

Figure 2.6 Intermetallic thickness (CH furnace heating, ID induction heating)

The growth of the intermetallic phases is governed by chemical reactions at the interfaces and interdiffusion between different phases [25, 26]. The phase constituents of the intermetallic layer (zone II) were quite different depending on the heating method and dwell time, as listed in Table 2.3. The phase constituents were determined by comparing the composition obtained from the SEM–EDS analysis to Al–Fe equilibrium phase diagrams.

The coating of the EA-0 specimen (dwell time of 0 s) has an intermetallic layer composed of Fe_4Al_{13}, $FeAl_3$, and Fe_2Al_5 intermetallics, while the Fe_4Al_{13} intermetallic appears as a main component of the intermetallic layer. Note that a thin bright layer of $FeAl_3/Fe_2Al_5$ was identified at the interface between the Fe_4Al_{13} layer and steel substrate. For the EA-10 specimen (dwell time of 10 s), the intermetallic phases are quite similar to those of the EA-0 specimen, except that the intermetallic layer became thicker. The circular islands in zone I of the EA-10 specimen were identified as the $FeAl_3$ intermetallic. Note that these intermetallic compounds, which have a relatively higher aluminum content, are reported to have a quite low fracture toughness of 1 MPa $m^{1/2}$ and high hardness of 900–1150 HV0.05 [27]. Due to the inherent brittleness, these intermetallic compounds may promote the formation and propagation of cracks in the coating, which eventually cause damage of the steel substrate.

The coating of the EA-25 specimen (dwell time of 25 s) exhibits complete intermetallic evolution, as mentioned above. A sandwiched FeAl intermetallic having a high iron content was observed between the aluminum-rich intermetallic Fe_2SiAl_7 and steel substrate, while a very thin layer of $FeAl_2$ intermetallic was identified along the interface between the FeAl and Fe_2SiAl_7 intermetallics. The FeAl phase possesses a high fracture toughness of up to 26 MPa $m^{1/2}$ and low hardness of 300–650 HV0.05 [28]. This intermetallic is reported to counteract crack formation in the coating [27].

This result suggests that the modified EA rapid heating effectively completed evolution of the intermetallic phases with a dwell time of 25 s and induced a beneficial intermetallic layer in the coating–substrate interface. The effectiveness of the modified EA rapid heating process may be due to the athermal effect of the electric current (in addition to the well-known resistance heating effect) on the mobility of atoms, as reported in the studies of the effect of electric current on the recrystallization kinetics [29] and the diffusion during electrically assisted brazing [30]. By further accelerating the mobility of atoms in the coating and steel substrate, modified EA rapid heating can expedite diffusion between the Al–Si coating and boron steel substrate.

Table 2.3 Phase constituents of intermetallic layer (zone II) *

Specimen	EDS point	Thickness (μm)	Phase constituents	Chemical composition (at. %)		
				Fe	Si	Al
As-received	A	2.19 ± 0.68	Fe_2SiAl_7	19.42	12.82	67.75
CH	A	3.75 ± 0.13	$FeAl_3$	21.01	12.42	66.58
ID	A	3.24 ± 0.58	Al rich	12.51	17.40	70.09
EA-0	A	5.04 ± 0.66	Fe_4Al_{13}	18.39	13.13	68.47
	B			23.39	9.85	66.75
EA-10	A	6.51 ± 0.26	Fe_4Al_{13} or $FeAl_3$	18.39	13.13	68.47
	B		Fe_2Al_5	23.39	9.85	66.75
EA-25	A	9.56 ± 0.8	Fe_2SiAl_7	20.87	11.05	68.09
	B		$FeAl_2$	31.68	4.47	63.85
	C		FeAl	51.08	1.35	47.56

*Zone I and zone III are always the Al-Si coating and the steel substrate, respectively; no zone I remains in case of EA-25

2.4 Summary

Modified electrically assisted (EA) rapid heating of Al–Si coated hot stamping steel was suggested, and the intermetallic evolution in the coating during the heating process was experimentally investigated. As shown in the result of the microstructural analysis, the modified EA rapid heating effectively completed evolution of intermetallic phases with a dwell time of 25 s and induced a ductile intermetallic phase, which contributes to prevent crack formation in the coating. The completion of intermetallic evolution was clearly impossible for conventional furnace or induction heating with the same dwell time. The effectiveness of EA rapid heating may be due to the athermal effect of the electric current on the mobility of atoms, in addition to the well-known resistance heating effect. The modified EA rapid heating suggested in the present study provides a clear technical advantage over conventional heating methods. By effectively and significantly reducing the heating time necessary to stabilize the Al–Si coating, the cycle time of the hot stamping process can be significantly reduced. Also, the modified EA rapid heating process provides an additional technical advantage in that partial heating can be easily achieved by properly placing the electrodes as demonstrated in the present study.

2.5 References for chapter 2

[1] Mori K, Akita K, Abe Y. Springback behaviour in bending of ultra-high-strength steel sheets using CNC servo press. International Journal of Machine Tools and Manufacture. 2007 Feb 1;47(2):321-5.

[2] Mori K, Okuda Y. Tailor die quenching in hot stamping for producing ultra-high strength steel formed parts having strength distribution. CIRP annals. 2010 Jan 1;59(1):291-4.

[3] Kim H, Han S, Yan Q, Altan T. Evaluation of tool materials, coatings and lubricants in forming galvanized advanced high strength steels (AHSS). CIRP annals. 2008 Jan 1;57(1):299-304.

[4] Naderi M, Ketabchi M, Abbasi M, Bleck W. Analysis of microstructure and mechanical properties of different high strength carbon steels after hot stamping. Journal of Materials Processing Technology. 2011 Jun 1;211(6):1117-25.

[5] Merklein M, Lechler J, Geiger M. Characterisation of the flow properties of the quenchenable ultra high strength steel 22MnB5. CIRP annals. 2006 Jan 1;55(1):229-32.

[6] Merklein M, Lechler J. Investigation of the thermo-mechanical properties of hot stamping steels. Journal of materials processing technology. 2006 Jul 3;177(1-3):452-5.

[7] Geiger M, Merklein M, Hoff C. Basic investigations on the hot stamping steel 22MnB5. InAdvanced Materials Research 2005 (Vol. 6, pp. 795-804). Trans Tech Publications Ltd.

[8] Manzenreiter T, Rosner M, Kurz T, Brugger G, Kelsch R, Hartmann D, Sommer A. Challenges, and advantages in usage of zinc-coated, press-hardened components with tailored properties. BHM Berg-und Hüttenmännische Monatshefte. 2012 Mar 1;157(3):97-101.

[9] Fan DW, De Cooman BC. State-of-the-Knowledge on coating systems for hot stamped parts. Steel research international. 2012 May;83(5):412-33.

[10] Zhao K, Chang Y, Hu P, Wu Y. Influence of rapid cooling pretreatment on microstructure and mechanical property of hot stamped AHSS part. Journal of Materials Processing Technology. 2016 Feb 1; 228:68-75.

[11] Suehiro M, Kusumi K, Miyakoshi T, Maki J, Ohgamt M. Properties of aluminum-coated steels for hot stamping. Nippon Steel, Tokyo (2003).

[12] Kolleck R, Veit R, Merklein M, Lechler J, Geiger M. Investigation on induction heating for hot stamping of boron alloyed steels. CIRP annals. 2009 Jan 1;58(1):275-8.

[13] Mori KI, Maeno T, Yamada H, Matsumoto H. 1-Shot hot stamping of ultra-high strength steel parts consisting of resistance heating, forming, shearing and die

quenching. International Journal of Machine Tools and Manufacture. 2015 Feb 1; 89:124-31.

[14] Allély C, Dosdat L, Clauzeau O, Ogle K, Volovitch P. Anticorrosion mechanisms of aluminized steel for hot stamping. Surface and Coatings Technology. 2014 Jan 15; 238:188-96.

[15] Borsetto F, Ghiotti A, Bruschi S. Investigation of the high strength steel Al-Si coating during hot stamping operations. InKey Engineering Materials 2009 (Vol. 410, pp. 289-296). Trans Tech Publications Ltd.

[16] Windmann M, Röttger A, Theisen W. Formation of intermetallic phases in Al-coated hot-stamped 22MnB5 sheets in terms of coating thickness and Si content. Surface and Coatings Technology. 2014 May 15; 246:17-25.

[17] Gui ZX, Liang WK, Liu Y, Zhang YS. Thermo-mechanical behavior of the Al–Si alloy coated hot stamping boron steel. Materials & Design. 2014 Aug 1; 60:26-33.

[18] Wang K, Jin Y, Zhu B, Zhang Y. Investigation on cracking characteristics of Al–Si coating on hot stamping boron steel parts based on surface strain analysis. Surface and Coatings Technology. 2017 Jan 15; 309:282-94.

[19] Gui ZX, Liang WK, Zhang YS. Formability of aluminum-silicon coated boron steel in hot stamping process. Transactions of Nonferrous Metals Society of China. 2014 Jun 1;24(6):1750-7.

[20] Łyszkowski R, Bystrzycki J. Hot deformation and processing maps of a Fe–Al intermetallic alloy. Materials characterization. 2014 Oct 1; 96:196-205.

[21] Davies J, Simpson P. Induction heating handbook. London: McGraw-Hill; 1979.

[22] Eggeler G, Auer W, Kaesche H. On the influence of silicon on the growth of the alloy layer during hot dip aluminizing. Journal of Materials Science. 1986 Sep 1;21(9):3348-50.

[23] Cheng WJ, Wang CJ. Effect of silicon on the formation of intermetallic phases in aluminide coating on mild steel. Intermetallics. 2011 Oct 1;19(10):1455-60.

[24] Cheng WJ, Wang CJ. Microstructural evolution of intermetallic layer in hot-dipped aluminide mild steel with silicon addition. Surface and Coatings Technology. 2011 Jun 25;205(19):4726-31.

[25] Fan DW, De Cooman BC. Formation of an aluminide coating on hot stamped steel. ISIJ international. 2010 Nov 15;50(11):1713-8.

[26] Bouayad A. Ch. Gerometta, A. Belkebir, A. Ambari. Mater. Sci. Eng. A. 2003; 363:53.

[27] Kobayashi S, Yakou T. Control of intermetallic compound layers at interface between steel and aluminum by diffusion-treatment. Materials science and engineering: A. 2002 Dec 15;338(1-2):44-53.

[28] Bouayad A, Gerometta C, Belkebir A, Ambari A. Kinetic interactions between solid iron and molten aluminium. Materials Science and Engineering: A. 2003 Dec 20;363(1-2):53-61.

[29] Windmann M, Röttger A, Theisen W. Phase formation at the interface between a boron alloyed steel substrate and an Al-rich coating. Surface and Coatings Technology. 2013 Jul 15; 226:130-9.

[30] Park JW, Jeong HJ, Jin SW, Kim MJ, Lee K, Kim JJ, Hong ST, Han HN. Effect of electric current on recrystallization kinetics in interstitial free steel and AZ31 magnesium alloy. Materials Characterization. 2017 Nov 1;133:70-6.

Chapter 3

The effect of pre-strain and subsequent electrically-assisted annealing on the mechanical behaviors of two different aluminum alloys

3.1 Introduction

Lightweight materials are widely used in the automotive industry for energy conservation and due to environmental considerations [1]. Among the many lightweight materials available, aluminum alloys become promising candidates due to their unique properties such as high strength-to-weight ratio and excellent corrosion resistance [2,3]. More specifically, non-heat treatable Al-Mg alloys and heat treatable Al-Mg-Si alloys have the potential for use in automotive body panel applications [4]. However, in comparison with conventional ferrous alloys, limited formability of those aluminum alloys is a considerable impediment to using them to manufacture complex components at room temperature.

To address the limited formability of aluminum alloys, researchers have investigated various manufacturing processes. For example, a preform annealing method (dual stage forming) to produce stamped sheet metal panels using aluminum alloys has been proposed [5-7]. In dual stage forming, an aluminum alloy sheet is preformed to a substantial amount of strain without fracture. Then, the

preformed part is subjected to either partial or entire annealing to remove work hardening through static recovery or recrystallization. The second stage involves further plastically deforming the part from the preforming stage to achieve the final part geometry. Li *et al.* [8] reported that 40% total effective elongation was achieved with 20% pre-strained non-heat treatable aluminum alloys after annealing. Wang *et al.* [9] also proved that the ductility of heat treatable aluminum alloys was improved by two-stage forming with annealing. According to Fang et al. [10], a desired grain structures for typical applications of non-heat treatable aluminum alloy could be simply achieved by a proper combination of cold deformation and subsequence annealing process. Although the dual stage forming method is effective and clearly improves formability, it is still far from being entirely satisfactory, since it is time-consuming to perform and requires a large workspace for annealing between forming stages. The forming process must be stopped, and the part needs to be transferred between the forming and heating areas.

For these reasons, dual stage forming with electrically assisted (EA) annealing was proposed as an alternative to conventional dual stage forming. Dual stage forming with EA annealing (or simply, EA dual stage forming) is a new manufacturing process based on the combination of the athermal effect of electricity and the thermal effect of resistance heating on the material properties of metals (electroplasticity) [8-16]. In EA dual stage forming, electric current is

applied to produce rapid EA annealing to the material deformed in the preforming stage [17].

EA dual stage forming has various technical advantages over conventional dual stage forming. As reported in recent studies [13,17], the athermal effect of electric current can significantly reduce process time at elevated temperatures to annihilate strain hardening from the preforming stage. Also, rapid heating to the target temperature by resistance heating can further reduce the total process time. In addition, the annealing facility can be simplified and consequently workspace for annealing can be significantly reduced. Finally, by careful placement of electrodes, the workpiece can be partially heated to facilitate optimization of the mechanical properties of the formed part.

However, as reported in Kim *et al.* [18], the effect of electric current on the mechanical properties of metallic materials can differ according to alloy composition and heat treatment conditions. Depending on the given metallic material, electric current can increase formability, which is desirable, or accelerate formation of microstructural damages, which is undesirable [19]. Therefore, in the design of EA dual stage forming of aluminum alloys, the effect of electric current on the post-EA annealing mechanical behavior of different aluminum alloys needs to be evaluated. In the present study, we experimentally investigated and compared the post-EA annealing mechanical behaviors of two different pre-strained commercial aluminum alloys.

3.2 Experimental procedures

Commercially available 1.2 mm-thick non-heat treatable Al-Mg alloy (5182-O) sheets and 1.6 mm-thick heat treatable Al-Mg-Si alloy (6061-T6) sheets were used in the experiment. The chemical compositions of these alloys are listed in Table 3.1. Tensile specimens with a gauge width of 12.5 mm and a gauge length of 50 mm were prepared along the rolling direction according to ASTM-E08 [20].

Table 3.1 The mechanical compositions of materials

Chemical compositions							
Aluminum alloys*	**Alloying element (wt%)**						
	Si	**Fe**	**Cu**	**Mn**	**Mg**	**Cr**	**Zn**
6061 – T6	0.4	0.7	0.15	0.15	0.8	0.04	0.25
5182 – O	0.2	0.35	0.15	0.2	4.0	0.1	0.25

* Al is at balance

As schematically described in Fig. 3.1, the specimen was first pre-strained (deformation stage I) in quasi-static uniaxial tension using a universal testing machine (DTU 900 MHN, Daekyung technology, South Korea) to a prescribed strain and automatically unloaded. The pre-strained specimen was then subjected to short duration EA annealing followed by air cooling for 3 min. In deformation stage II, simple quasi-static tension was applied to the EA annealed specimen until fracture. For both stages I and II, the specimen was deformed with a constant displacement rate of 3 mm/min (engineering strain rate of 10^{-3} s^{-1} based on the original gauge length of the specimen). A non-contact high-resolution laser extensometer (LX500, MTS systems corporation, USA) was used to measure the displacement.

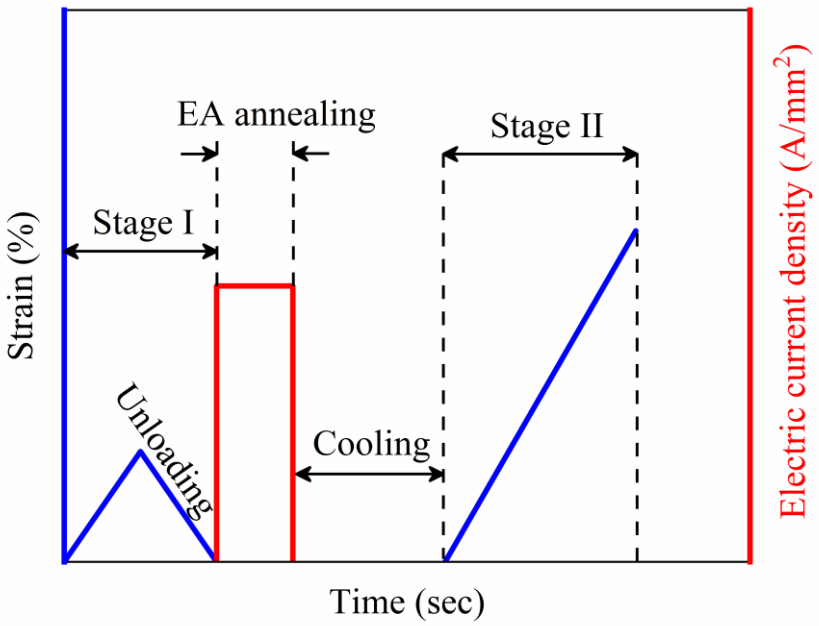

Figure 3.1 A schematic of the experimental procedure. The blue and red lines indicate the strain state and the applied electric current density, respectively

Experimental set-up for EA annealing comprised a programmable DC power supply (Vadal SP–1000U welder, Hyosung, South Korea), electric cables, two copper electrodes, and an infrared thermal imaging camera (FLIR-T440, FLIR Systems, Oregon, USA), as shown in Fig. 3.2. As illustrated in the inset of Fig. 3.2, a sliding mechanism was employed in EA annealing. Bakelite insulators were used to ensure that electric current was applied only to the specimen for the safety. Bakelite insulators connected to electrodes slid along the length direction of the specimen to avoid bending of the specimen due to thermal expansion during EA annealing. The temperature history and temperature profile along the length of the specimen were monitored during EA annealing by the infrared thermal imaging camera. A high-temperature black thermal paint was sprayed on one surface of the specimen to stabilize emissivity. The emissivity used for infrared thermal imaging was calibrated based on preliminary tests using a K-type thermocouple.

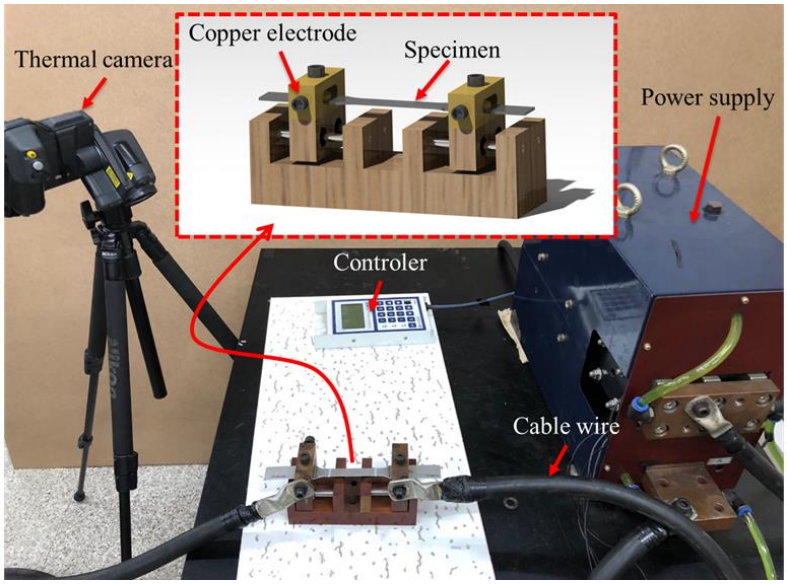

Figure 3.2 A schematic of experimental set-up for EA annealing

In the present study, two different pre-strain levels (65%ε_{UTS} and 85%ε_{UTS}) were selected, as listed in Table 3.2. The strain of ε_{UTS} is the engineering strain at the maximum uniform elongation. Therefore, the pre-strains of 65%ε_{UTS} and 85%ε_{UTS} correspond to 65% and 85% of the engineering strain at maximum uniform elongation, respectively. For each pre-strain level, three different true electric current densities (100, 125, and 140 A/mm^2) based on the actual cross-sectional area of the pre-strained specimen were applied to the pre-strained specimen to induce EA annealing. For simplicity, the duration of electric current was set to the constant of 0.75 sec for all experiments. To verify the repeatability of the result, at least three specimens were tested for each parameter set.

Table 3.2 The experimental parameters

Material	**Pre-strain level**	**Engineering strain (%)**	**True electric current density* (A/mm^2)**
5182-O	As-received (No pre-strain, No current)		
	65% ε_{UTS}	12	No EA (No current)
			100
			125
			140
	85% ε_{UTS}	15.7	No EA (No current)
			100
			125
			140
6061-T6	As-received (No pre-strain, No current)		
	65% ε_{UTS}	6	No EA (No current)
			100
			125
			140
	85% ε_{UTS}	7.9	No EA (No current)
			100
			125
			140

*Duration of 0.75 sec

In addition to evaluation of mechanical properties during reloading after EA annealing, microstructural analyses of cross-sectional samples of the as-received specimens and the pre-strained specimens prior to and after EA annealing were conducted using an X-ray diffractometer (D8-Advanced, Brucker miller co., Boston, MA, USA) with a Cu radiation source operating at 40 kV and an FE-SEM (Quanta 200F FEI, Hillsboro, OR, USA) equipped with an EBSD system (Digiview4, EDAX, Mahwah, NJ, USA). Samples for microstructural analyses were prepared using a standard metallographic grinding technique followed by electropolishing with 10% perchloric acid and 90% ethanol at a temperature of about -20°C and voltage of 20 V.

3.3 Initial properties of as-received, and pre-strained specimen: mechanical behavior, and microstructure

As expected, the engineering stress-strain curves of the tensile tests (Figs. 3.3(a) and (b)) show that the reloading curves of pre-strained specimens without EA annealing went back to and followed the baseline curves of the as-received specimens (no pre-strain) in general for both selected aluminum alloys, when the reloading curves were constructed based on the initial gauge length and initial cross-sectional area prior to pre-strain.

For the 6061-T6 alloy, a modest bump was observed in the flow stress of the reloading curves on account of strain aging [21]. Transformation of the reloading curves in Figs. 3.3(a) and (b) to engineering stress-strain curves during stage II (or stage II engineering stress-strain curves, Figs. 3.3(c) and (d)) based on the gauge length and cross-sectional area at the initiation of reloading clearly demonstrates the effect of pre-strain (strain hardening) on the mechanical behavior of both selected aluminum alloys.

(a)

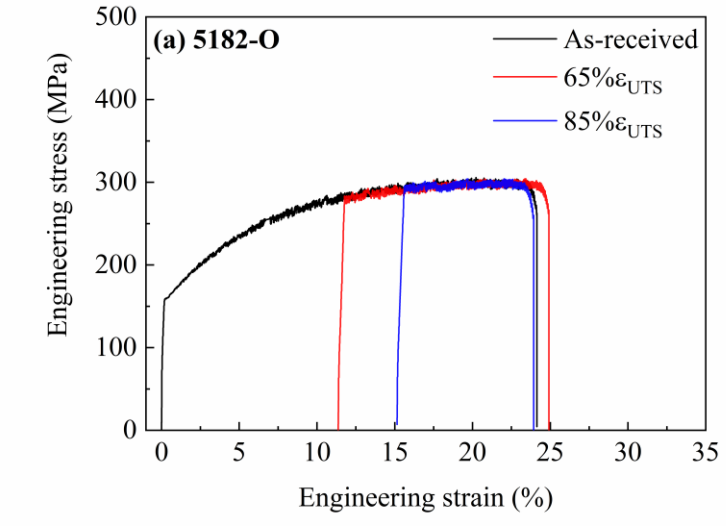
(a) 5182-O
As-received
65%ε_UTS
85%ε_UTS
Engineering stress (MPa)
Engineering strain (%)
0
100
200
300
400
500
0
5
10
15
20
25
30
35

(b)

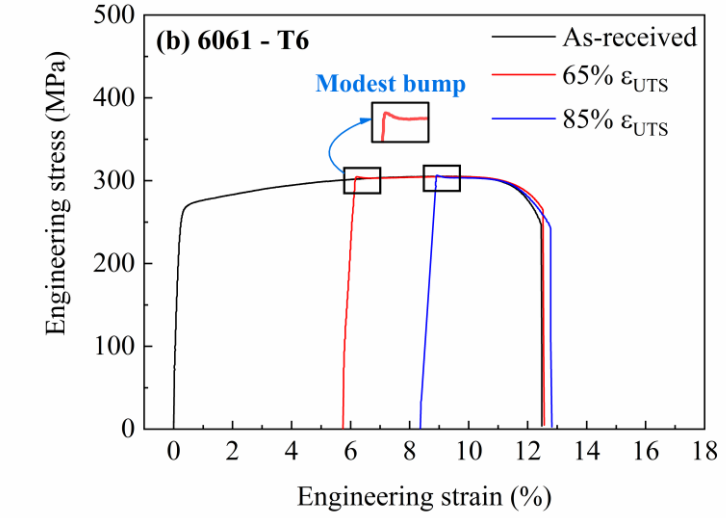
(b) 6061 - T6
As-received
65% ε_UTS
85% ε_UTS
Modest bump
Engineering stress (MPa)
Engineering strain (%)
0
100
200
300
400
500
0
2
4
6
8
10
12
14
16
18

(c)

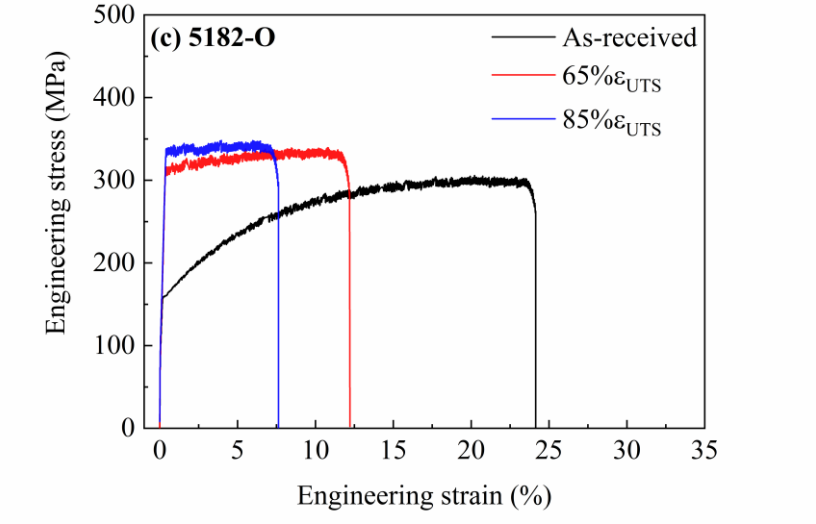

(d)

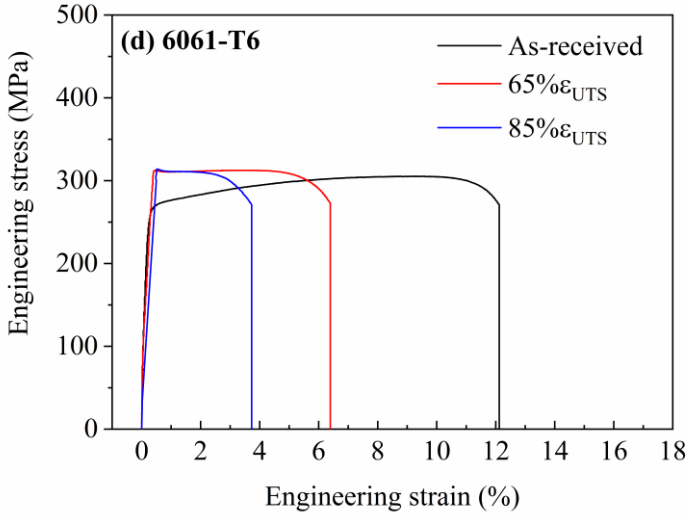

Figure 3.3 As-received and reloading without EA annealing engineering stress-strain curves of (a, c) 5182-O aluminum alloys, and (b, d) 6061-T6 aluminum alloys: constructed based on the initial gauge length and initial cross-sectional area prior to pre-strain

Broadening of X-ray diffraction peaks indicates the lattice distortions, such as dislocations accumulation in the crystal. In analysis of the profiles of diffraction peaks, the full width at half maximum (FWHM) is sensitive to variations in microstructure under the same instrumental conditions and finite crystallite size [22]. In the present study, we assumed that the instrumental broadening contribution of the diffractometer was consistent for every measurement due to identical operational conditions. We also assumed that the finite crystallite domain size was entirely equivalent to the tested specimens. Based on these assumptions, FWHM analysis was used to evaluate lattice distortions, including dislocations.

For both selected aluminum alloys, pre-strain induced an increase in FWHM, as shown in Figs. 3.4(a) and (b). The results indicate comparable distortion of the individual grains by plastic deformation in stage I. As the magnitude of the pre-strain increased, dislocation density increased due to dislocation multiplication or formation of new dislocations. Therefore, it is logical that the FWHMs of the 85%ε_{UTS} pre-strained specimens (specimens pre-strained to 85%ε_{UTS}) were higher than those of the 65%ε_{UTS} pre-strained specimens (specimens pre-strained to 65%ε_{UTS}) for both aluminum alloys. The inverse pole figure (IPF) maps of the as-received and pre-strained specimens (Figs. 3.5(a) and (b)) show equiaxed and uniformly distributed grains in both aluminum alloys. Average grain sizes of the as-received specimens were measured as 16±7 μm and 24±10 μm for the 5182-O alloy and the 6061-T6 alloy, respectively. No specific change in grain size was

observed for either pre-strain level (65%ε_{UTS} and 85%ε_{UTS}) of either aluminum alloy.

(a)

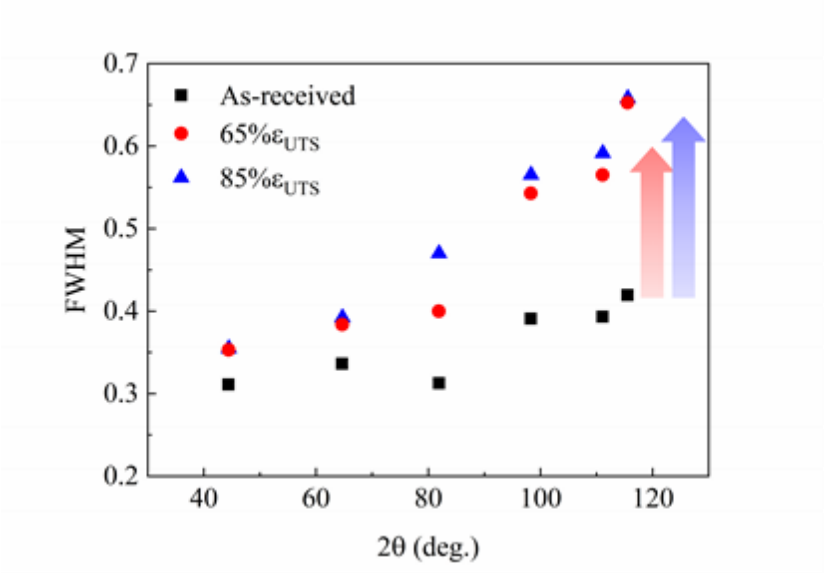

(b)

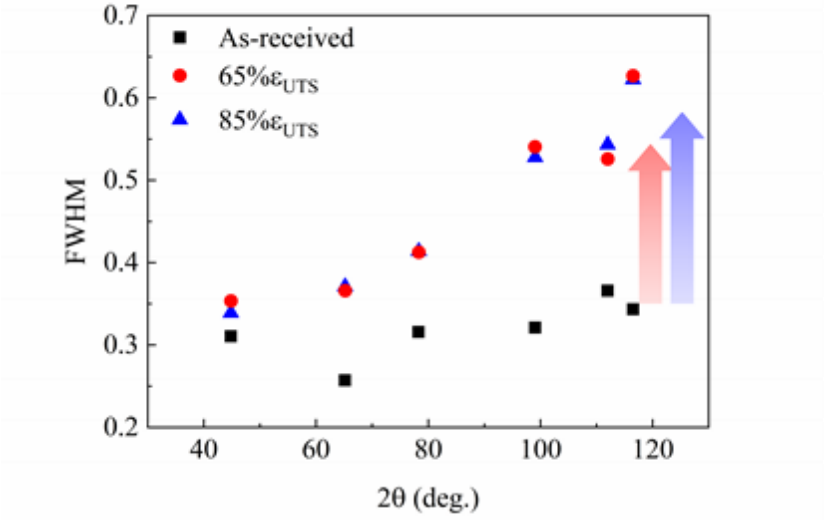

Figure 3.4 The effect of pre-strain to the FWHM profiles of (a) 5182-O, and (b) 6061-T6 aluminum alloys

(a)

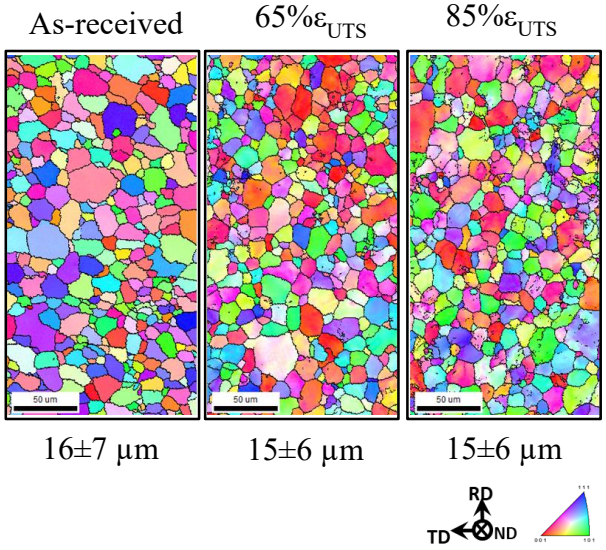

(b)

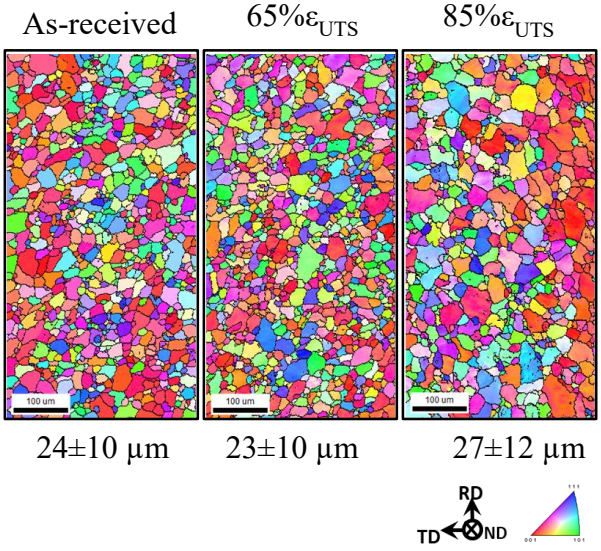

Figure 3.5 Inverse pole figure maps of as received and pre-strained specimens prior to EA annealing for (a) 5182-O, and (b) 6061-T6 aluminum alloys

3.4 Temperature during EA annealing

Due to resistance heating, heat was generated instantly in all tested specimens when electric current was applied during EA annealing. However, with the subsecond duration used in the present study, exposure of the specimen to an elevated temperature was relatively short in comparison with conventional heat treatment, which can easily be longer than 20 min [23]. For example, as shown in Fig. 3.6(a), with a true electric current density of 140 A/mm^2, the temperature of the 85%ε_{UTS} pre-strained specimen of the 6061-T6 alloy rapidly reached the peak temperature of 390°C in 0.75 sec and decreased to room temperature in 45 sec. The increase in true electric current density led to an increase in peak temperature (Fig. 3.6(a)). For each alloy, temperature responses (peak temperatures) to the applied electric current of specimens with different pre-strain levels were quite similar since the true electric current density was used (Fig. 3.6(b)). At the same true electric current density, the 5182-O alloy reached a higher temperature than the 6061-T6 alloy due to the former's higher electrical resistivity.

(a)

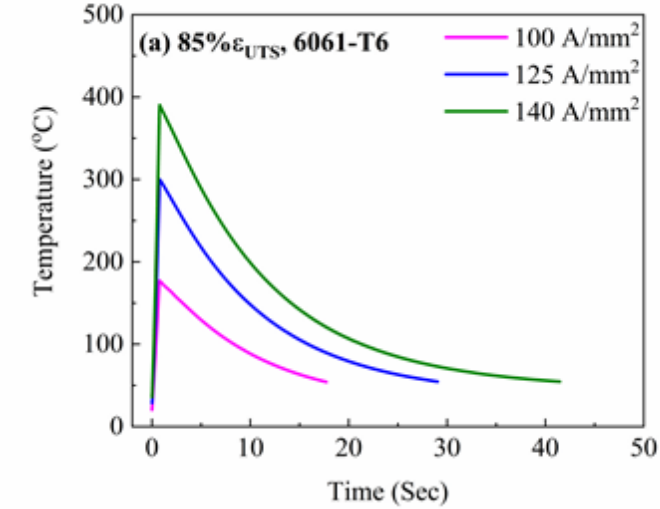
(a) 85%ε$_{UTS}$, 6061-T6
100 A/mm^2
125 A/mm^2
140 A/mm^2
Temperature (°C)
Time (Sec)
0
100
200
300
400
500
0
10
20
30
40
50

(b)

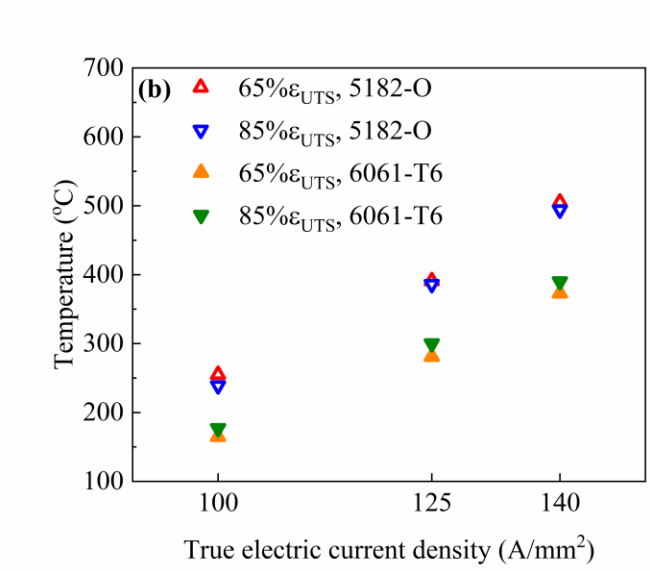
(b)
65%ε$_{UTS}$, 5182-O
85%ε$_{UTS}$, 5182-O
65%ε$_{UTS}$, 6061-T6
85%ε$_{UTS}$, 6061-T6
Temperature (°C)
True electric current density (A/mm^2)
100
200
300
400
500
600
700
100
125
140

(c)

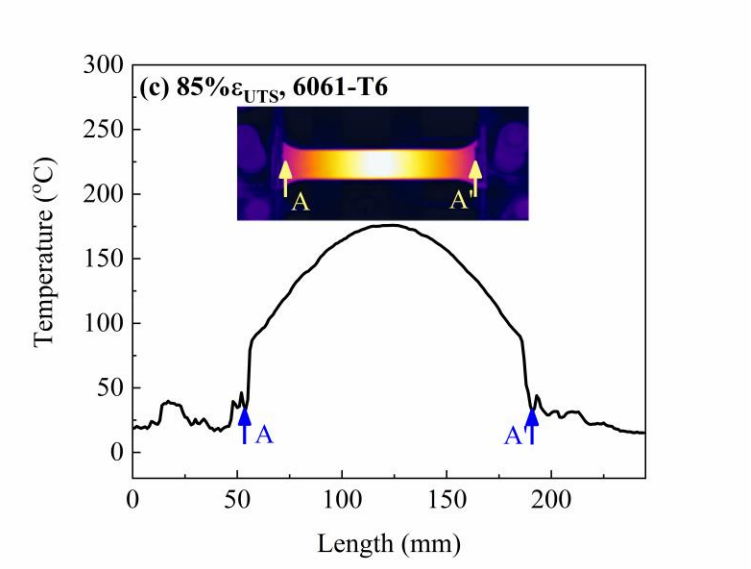

Figure 3.6(a) Temperature histories of 85%ε_{UTS} pre-strained 6061-T6 specimens subjected to EA annealing, (b) average temperature peaks as a function of true electric current density of pre-strained specimens during EA annealing, and (c) temperature profile of 85%ε_{UTS} pre-strained 6061-T6 specimen subjected to 100 A/mm^2 of electric current density

3.5 Mechanical properties after EA annealing

Reloading curves of the pre-strained specimens subjected to EA annealing (EA annealed specimens) were also transformed into stage II engineering stress-strain curves based on the actual gauge length and cross-sectional area at initiation of reloading. Representative stage II engineering stress-strain curves in addition to the baseline engineering stress-strain curves of the as-received specimens are presented in Fig. 3.7. Using stage II engineering stress-strain curves, the post-EA annealing yield strength (or simply, the post-EA yield strength) and the post-EA annealing elongation (or simply, the post-EA elongation), as defined in Fig. 3.7(a), of the EA annealed specimens were compared with those of the pre-strained specimens without EA annealing.

(a)

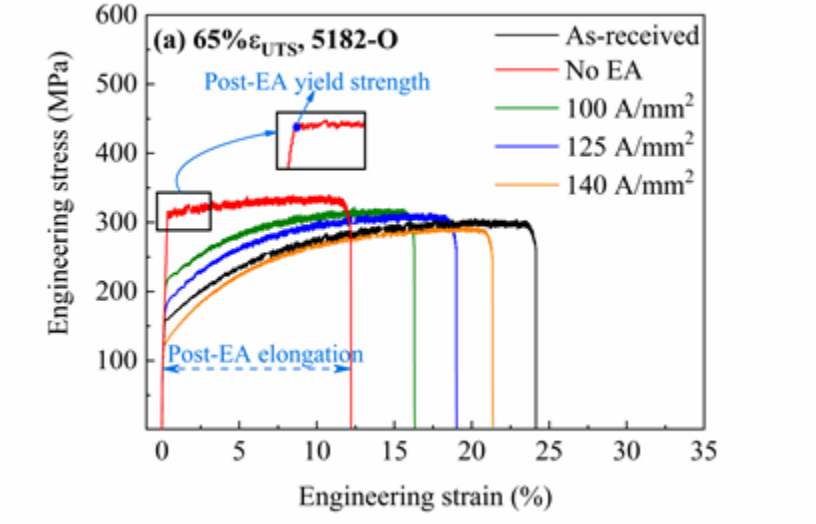
(a) 65%ε$_{UTS}$, 5182-O
Post-EA yield strength
Post-EA elongation
As-received
No EA
100 A/mm^2
125 A/mm^2
140 A/mm^2
Engineering stress (MPa)
Engineering strain (%)
600
500
400
300
200
100
0
5
10
15
20
25
30
35

(b)

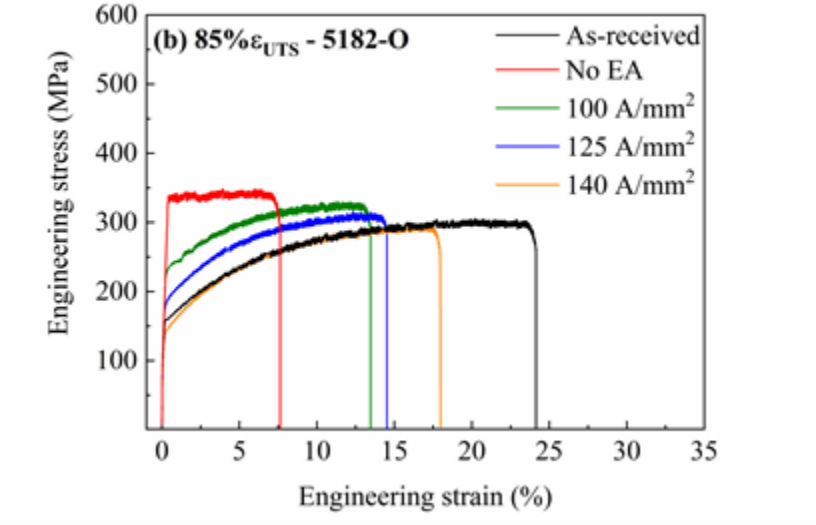
(b) 85%ε$_{UTS}$ - 5182-O
As-received
No EA
100 A/mm^2
125 A/mm^2
140 A/mm^2
Engineering stress (MPa)
Engineering strain (%)
600
500
400
300
200
100
0
5
10
15
20
25
30
35

(c)

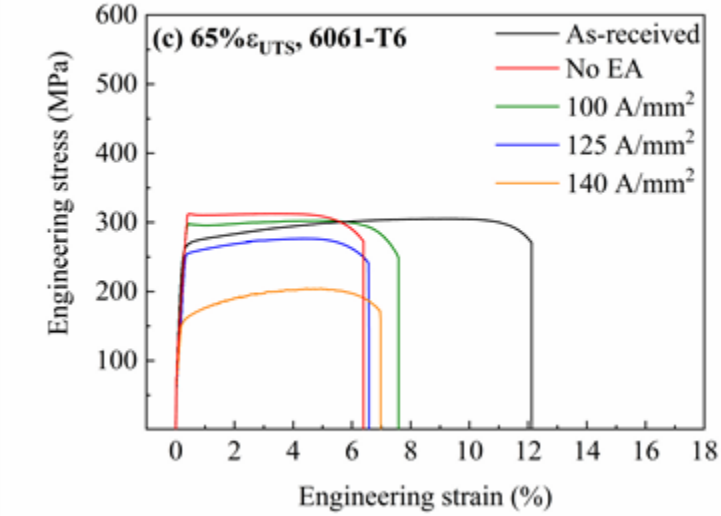

(d)

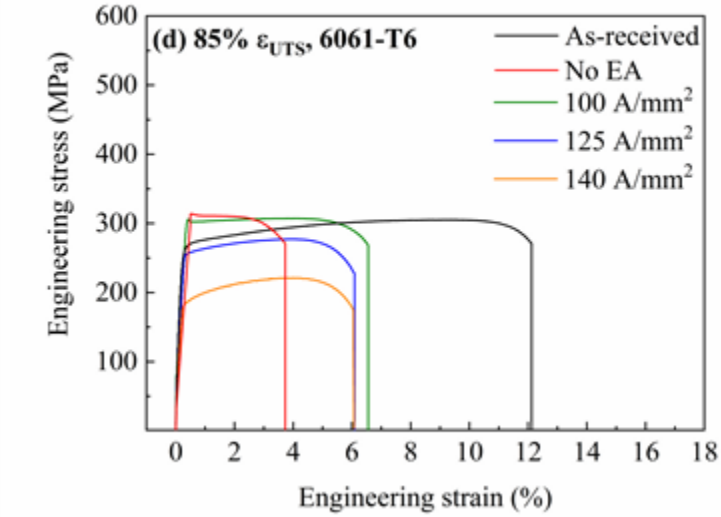

Figure 3.7 The engineering stress-strain curves based on the gauge length and cross-sectional area at initiation of reloading (stage II) of pre-strained specimens after EA annealing of 5182-O aluminum alloys: (a) 65%ε_{UTS}, and (b) 85%ε_{UTS}; 6061-T6 aluminum alloys: (c) 65%ε_{UTS}, and (d) 85%ε_{UTS}

Plots of post-EA yield strength as a function of the true electric current density suggest that annealing occurred to all the pre-strained specimens as a result of application of an electric current with a subsecond duration of 0.75 sec, as shown in Figs. 3.8(a) and (b). For both aluminum alloys, the post-EA yield strength clearly decreased after EA annealing. At the current density of 140 A/mm^2, the post-EA yield strength of both aluminum alloys for both pre-strain values became significantly lower than the baseline yield strength (no pre-strain) for each aluminum alloy. While both aluminum alloys showed a reduction in post-EA yield strength (i.e., reduction in work hardening) as a result of EA annealing, a comparison of the results shown in Figs. 3.8(a) and (b) suggests that the effect of electric current on post-EA yield strength, i.e., the extent of EA annealing, differed depending on the selected aluminum alloy. In the electric current density range selected in the present study, the post-EA yield strength of the 5182-O aluminum alloy decreased nearly linearly for both pre-strain levels. However, the post-EA yield strength of the 6061-T6 aluminum alloy showed a more rapid decrease as the electric current density increased from 125 to 140 A/mm^2, thus resulting in an almost non-linear decrease. Furthermore, while post-EA yield strength became lower than the baseline yield strength in the interval between the electric current densities of 125 A/mm^2 and 140 A/mm^2 for the 5182-O aluminum alloy, the post-EA yield strength of the 6061-T6 aluminum alloy was already lower than the baseline value at the electric current density of 125 A/mm^2.

(a)

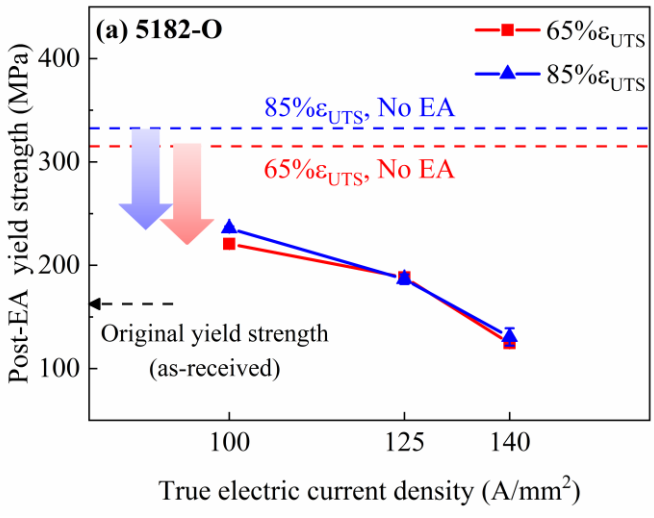

(b)

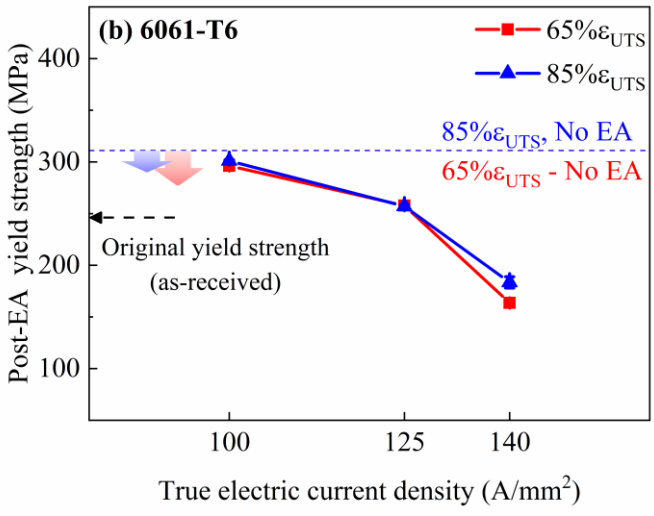

Figure 3.8 The effect of the electric current density on the post-EA yield strength of EA annealed (a) 5182-O, and (b) 6061-T6 pre-strained specimens. Each data point represents the average of three experimental results. Dispersion bars are based on the standard deviation

As a result of EA annealing, post-EA elongation of all pre-strained specimens increased in both aluminum alloys, as shown in Figs. 3.9(a) and (b). Note that post-EA elongation of the 85%ε_{UTS} pre-strained specimen was consistently lower than that of the 65%ε_{UTS} pre-strained specimen for both aluminum alloys due to the accumulation of more dislocations at the higher pre-strain level. Different effects of EA annealing on post-EA mechanical behavior (the mechanical behavior after EA annealing) according to the aluminum alloy were more pronounced in the post-EA elongation. For the pre-strained 5182-O specimens, as the electric current density increased, post-EA elongation clearly increased. Post-EA elongation of the pre-strained specimens did not fully regain their as-received elongation values, even though post-EA yield strength showed full annealing as the applied electric current density increased, as shown in Fig. 3.8(a).

Electric current had a different effect on the formability of the pre-strained 6061-T6 alloy. When an electric current density of 100 A/mm^2 was applied, the pre-strained 6061-T6 specimens exhibited an increase in post-EA elongation, which can be explained by EA annealing. However, a further increase in electric current density did not induce additional improvement of post-EA elongation in the pre-strained 6061-T6 specimens. Note that the reduction in post-EA yield strength at higher electric current densities for the pre-strained 6061-T6 specimens, as shown in Fig. 3.8(b), was significant. The different post-EA elongation recoveries

of the pre-strained 5182-O and 6061-T6 specimens will be discussed further in the section on microstructural analysis.

(a)

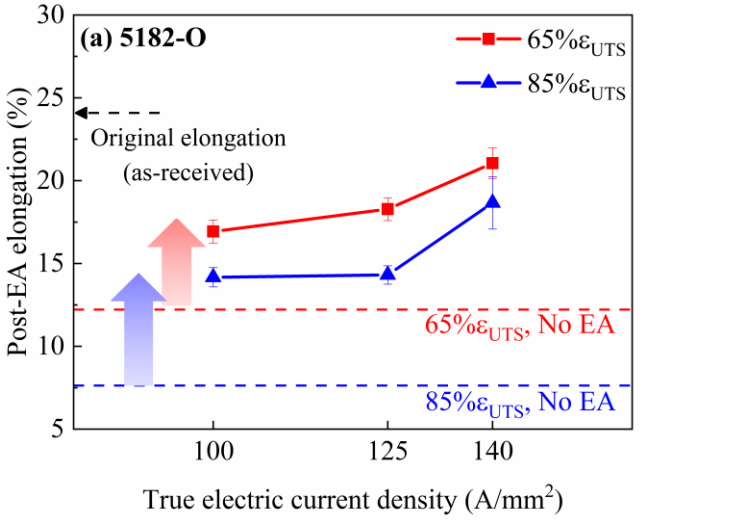

(b)

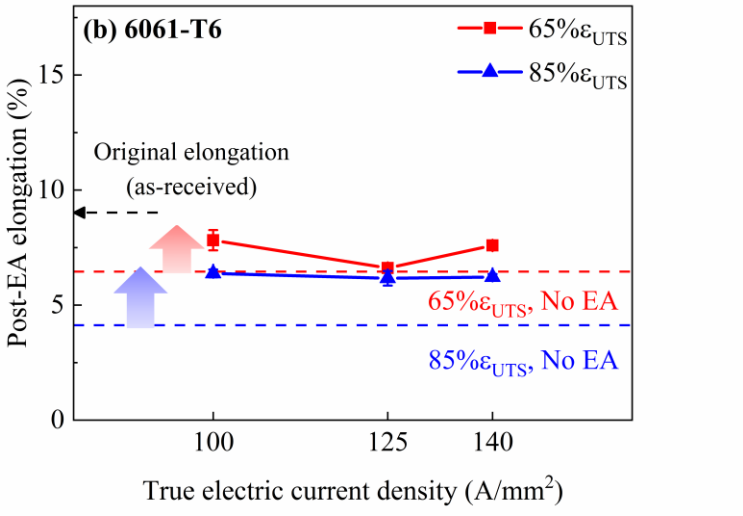

Figure 3.9 The effect of the electric current density on the post-EA elongation of EA annealed (a) 5182-O, and (b) 6061-T6 pre-strained specimens. Each data point represents the average of three experimental results. Dispersion bars are based on the standard deviation

A major objective of annealing in dual stage forming of an aluminum alloy is to retain the formability of the selected alloy to complete the entire forming process (stage I prior to annealing and stage II after annealing) without failure. Therefore, it is reasonable to evaluate the effect of EA dual stage forming on total achievable elongation until fracture. Total achievable elongation (or total achievable engineering strain) can be simply calculated by the summation of the total achievable displacements during stages I and II divided by the initial gauge length of the specimen, as presented in Figs. 3.10(a) and (b). For the 5182-O aluminum alloy, EA annealing led to a significant increase in total achievable elongation for both pre-strain levels. For example, the total achievable elongation of the 85%ε_{UTS} pre-strained specimen subjected to EA annealing with 140 A/mm^2 increased by about 1.5 times compared to that of the as-received specimen. Further, as the current density increased, the total achievable elongation increased for both pre-strain levels. This result is consistent with the effects of electric current on the mechanical properties of 5XXX series aluminum alloys reported previously [17]. In other words, as electric current density increased, the extent of EA annealing increased.

However, for the 6061-T6 aluminum alloy, even though the total achievable elongation was increased by EA annealing, the increase in total achievable elongation was less significant than that observed for the 5182-O aluminum alloy. More importantly, the magnitude of the increased total achievable elongation did

not change much as the electric current density increased. However, as will be discussed in detail below, microstructural analysis clearly revealed a higher extent of EA annealing with a higher electric current density for both aluminum alloys selected in the present study.

(a)

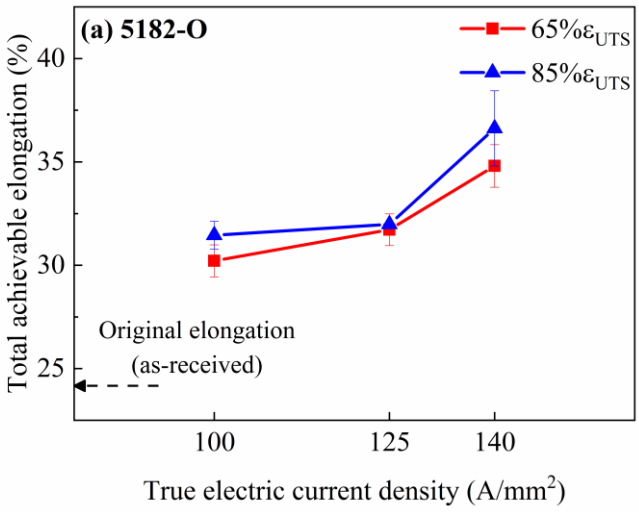

(b)

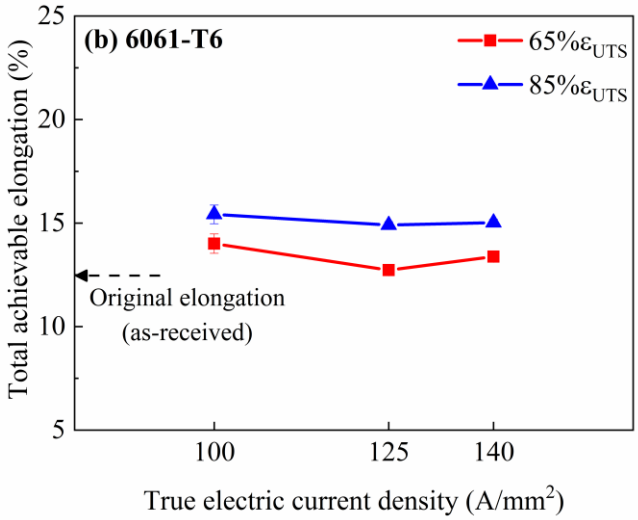

Figure 3.10 The effect of the electric current density on the total achievable elongation of (a) 5182-O, and (b) 6061-T6 pre-strained specimens subjected to EA annealing. Each data point represents the average of three experimental results. Dispersion bars are based on the standard deviation

3.6 Microstructures after EA annealing

To evaluate the effect of EA annealing on microstructure, EA annealed specimens were removed from the experiment without reloading. The FWHMs of the EA annealed specimens were then compared with those of the as-received and pre-strained specimens without EA annealing. As shown in Fig. 3.11, EA annealing clearly reduced the FWHMs of both aluminum alloys for both pre-strains levels (65%ε_{UTS} and 85%ε_{UTS}). For both aluminum alloys and both pre-strain levels, an increase in electric current density led to a further decrease in FWHM. The reduction in FWHM corresponds to the reduction in dislocation density [17]. Therefore, the results in Fig. 3.11 confirm that electric current induced annealing to all the pre-strained specimens of both aluminum alloys.

(a)

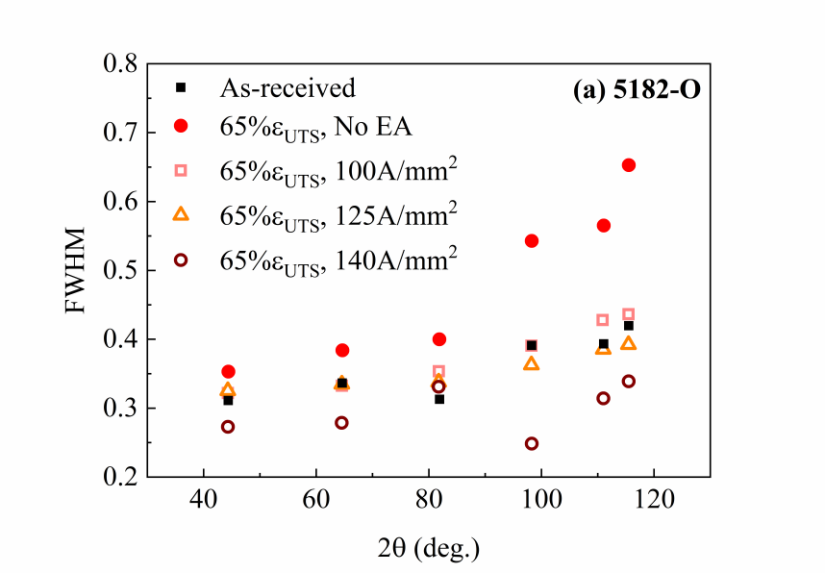
(a) 5182-O
As-received
65%ε$_{UTS}$, No EA
65%ε$_{UTS}$, 100A/mm^2
65%ε$_{UTS}$, 125A/mm^2
65%ε$_{UTS}$, 140A/mm^2
FWHM
2θ (deg.)
0.2
0.3
0.4
0.5
0.6
0.7
0.8
40
60
80
100
120

(b)

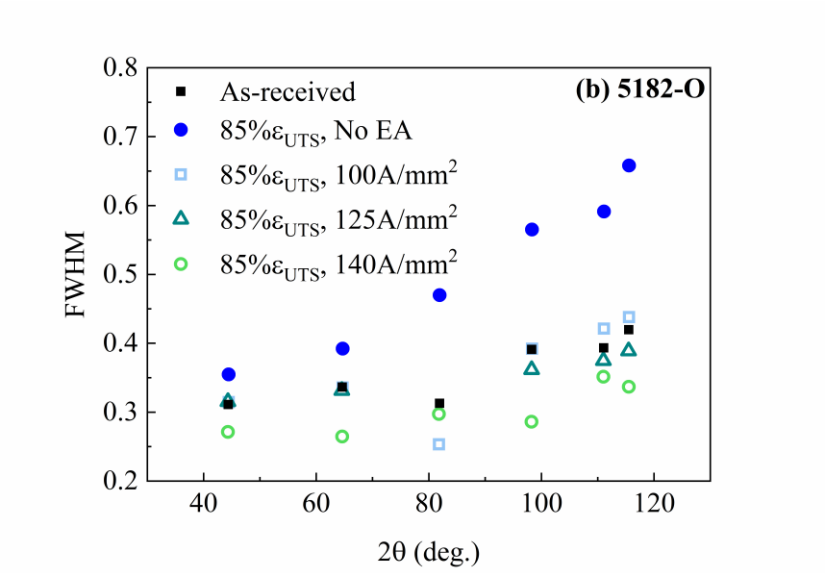
(b) 5182-O
As-received
85%ε$_{UTS}$, No EA
85%ε$_{UTS}$, 100A/mm^2
85%ε$_{UTS}$, 125A/mm^2
85%ε$_{UTS}$, 140A/mm^2
FWHM
2θ (deg.)
0.2
0.3
0.4
0.5
0.6
0.7
0.8
40
60
80
100
120

(c)

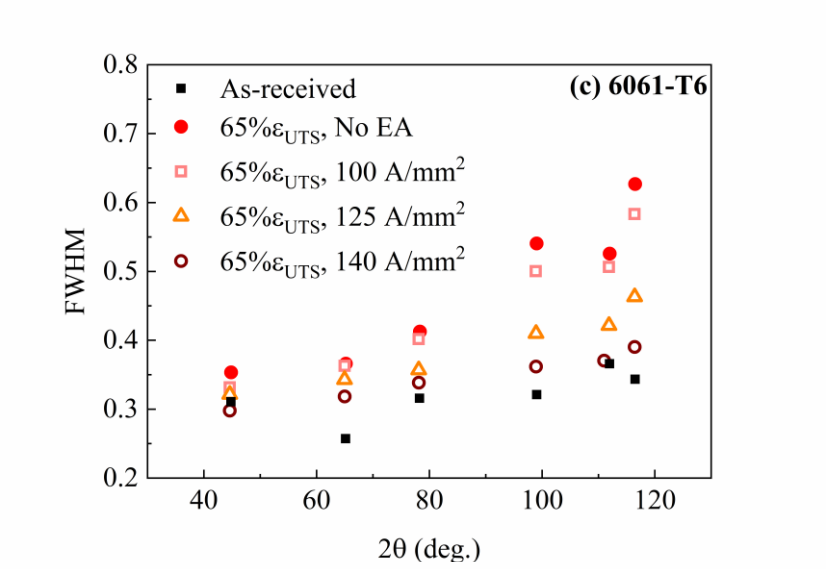

(d)

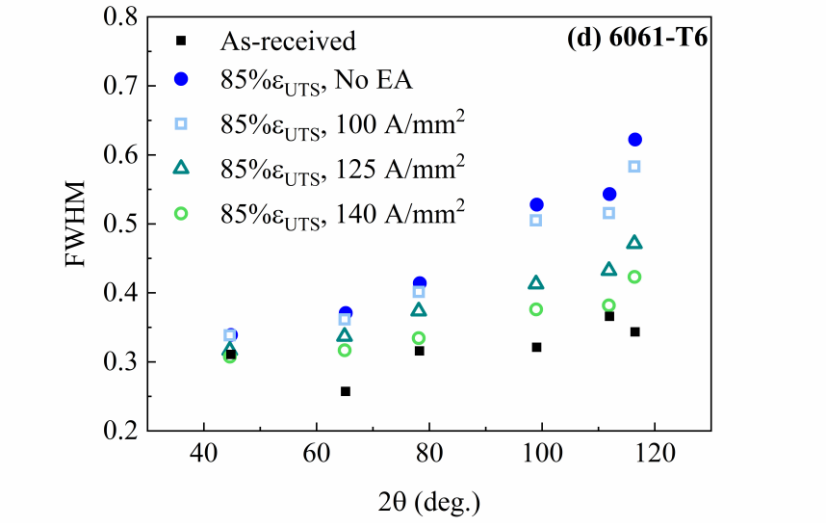

Figure 3.11 The effect of pre-strain and electric current density on the FWHM profile of 5182-O aluminum alloys: (a) 65%ε_{UTS}, and (b) 85%ε_{UTS}; 6061-T6 aluminum alloys: (c) 65%ε_{UTS}, and (d) 85%ε_{UTS}

For the 5182-O aluminum alloy, the FWHMs of both 65%ε_{UTS} and 85%ε_{UTS} pre-strained specimens subjected to EA annealing with 140 A/mm^2 became lower than that of the as-received specimen, as shown in Figs. 3.11(a) and (b). This suggests that full annealing, possibly to the extent of grain growth after recrystallization, occurred in the pre-strained specimens subjected to EA annealing with 140 A/mm^2, and these results are consistent with the tensile test results shown in Figs. 3.7(a) and (b).

However, for the 6061-T6 aluminum alloy, the FWHMs of both 65%ε_{UTS} and 85%ε_{UTS} pre-strained specimens subjected to EA annealing with 140 A/mm^2 were reduced to values similar to those of the as-received specimen, as shown in Figs. 3. 11(c) and (d), while the post-EA yield strengths of those specimens were significantly lower than the yield strength of the as-received specimen, as shown in Figs. 3.7(c) and (d). This discrepancy can be a result of the effect of high electric current density and the resultant peak temperature during EA annealing on the precipitates in the pre-strained 6061-T6 specimens. With the athermal effect of electric current, which can significantly accelerate the mobility of atoms [17,24,25], it is believed that some extent of solid solutioning occurred to the pre-strained 6061-T6 specimens during the EA annealing with 140 A/mm^2, even though the measured peak temperature during the EA annealing was lower than the general solid solution temperature (approximately 530°C) of 6061 aluminum alloys.

This argument is supported by the comparison (Fig. 3.12) of the stress-strain curve of the pre-strained specimen subjected to EA annealing with 140 A/mm^2 and that of the specimen (without pre-strain) subjected to 530°C conventional solid solution treatment in 1 hour using a furnace followed by water quenching. As shown in Fig. 3.12, serrations occurred in the stress-strain curve of the conventionally solid solution treated specimen, as a typical result of solid solution treatment [18]. The stress-strain curve of the pre-strained specimen subjected to EA annealing with 140 A/mm^2 also showed slight serrations, which strongly suggest the occurrence of some extent of solid solutioning. The fact that the post-EA yield strength (183 MPa) of the pre-strained specimen subjected to EA annealing with 140 A/mm^2 is between the yield strengths of the as-received (271 MPa) and the conventionally solid solution treated specimen (71 MPa) clearly corresponds to the occurrence of some extent of solid solutioning during the EA annealing. Hence, the results suggest that the electric current density of 140 A/mm^2 induced both annealing and solid solutioning in the pre-strained 6061-T6 alloy.

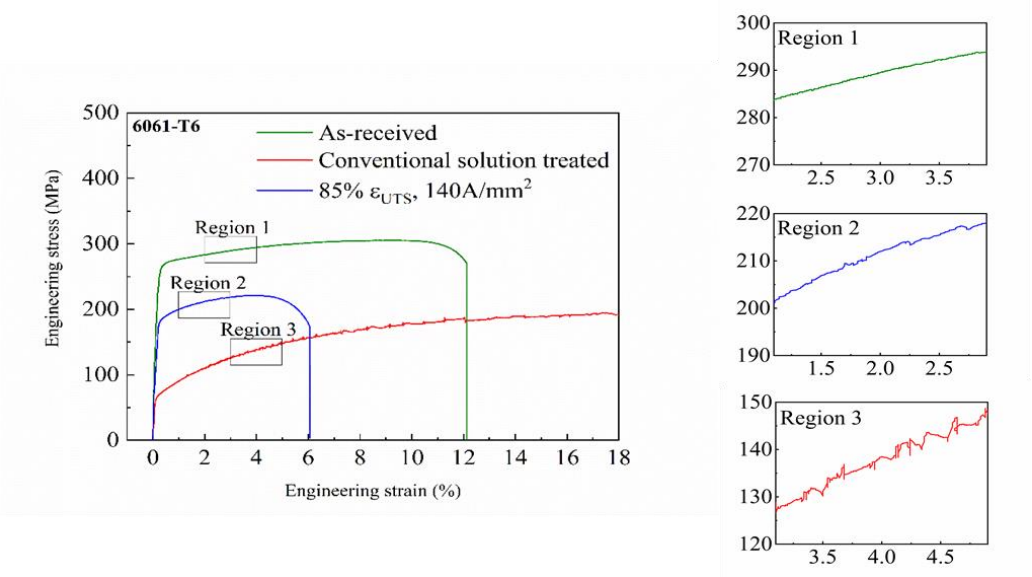

Figure 3.12 The engineering stress-strain curves of as-received and conventional solid solution treatment specimens compared to that of the 85%ε_{UTS} pre-strained specimen subjected to EA annealing with 140 A/mm^2: constructed based on the initial gauge length and initial cross-sectional area prior to pre-strain

IPF maps and the grains with 0° < GOS (grain orientation spread) < 1° are shown in Fig. 3.13 (5182-O aluminum alloy) and 3.14 (6061-T6 aluminum alloy). The recrystallized grains were identified based on the GOS value and they were distinguished from the deformed grains on the basis of a maximum GOS value of 1° in the present study.

Pre-strained specimens of the 5182-O aluminum alloy subjected to EA annealing with 140 A/mm^2 showed a microstructure with full recrystallization followed by grain growth (Fig. 3.12). These results are consistent with that the post-EA yield strengths at 140 A/mm2 was lower than the original (as-received) yield strength, as shown in Figs. 3.7(a), (b) and 3.8(a). The results shown in Figs. 3.12(a) and (b) also suggest that the effect of electric current on grain growth after recrystallization of pre-strained specimens depended on the pre-strain level. For the same true electric current density of 140 A/mm^2, the average grain size of the 65%ε_{UTS} pre-strained specimen (58 ± 22 μm) became much larger than that of the 85%ε_{UTS} pre-strained specimen (30 ± 10 μm) after EA annealing. This difference in grain size corresponds to the slightly lower post-EA yield strength of the 65%ε_{UTS} pre-strained specimen compared to that of the 85%ε_{UTS} pre-strained specimen, as shown in Fig. 3.8(a). This can be explained by the effect of pre-strain level (i.e., the extent of deformation) on recrystallized grain size during annealing [26]. As deformation increased, the rate of nucleation increased. In other words, the higher pre-strain level provided more nuclei per unit volume for new grains than

the lower pre-strain level. As a result, the new grains met with each other at the surface earlier due to a larger number of new grains, and consequently grain size became finer in the specimens with the higher pre-strain level.

While the occurrence of full annealing with grain growth in the pre-strained 5182-O aluminum alloy was confirmed by EBSD analysis, insufficient recovery of elongation by EA annealing (Fig. 3.9(a)) could be explained by the slightly non-uniform temperature distribution along the gage length during EA annealing. Electrodes contacting the specimen functioned as heat sinks, and regions with a lower temperature were unavoidable near the ends of gage section, as shown in Fig. 3.6(c). The lower temperature near the ends of the gage section led to a lower extent of EA annealing in those regions (nonuniform EA annealing along the length of gage section), since EA annealing is a combined result of the athermal effect of electric current and the elevated temperature resulting from resistance heating [17]. Nonuniform EA annealing along the length of the gage section reduced the actual length of the fully annealed region so that it was shorter than the length of the gage section of the pre-strained specimen.

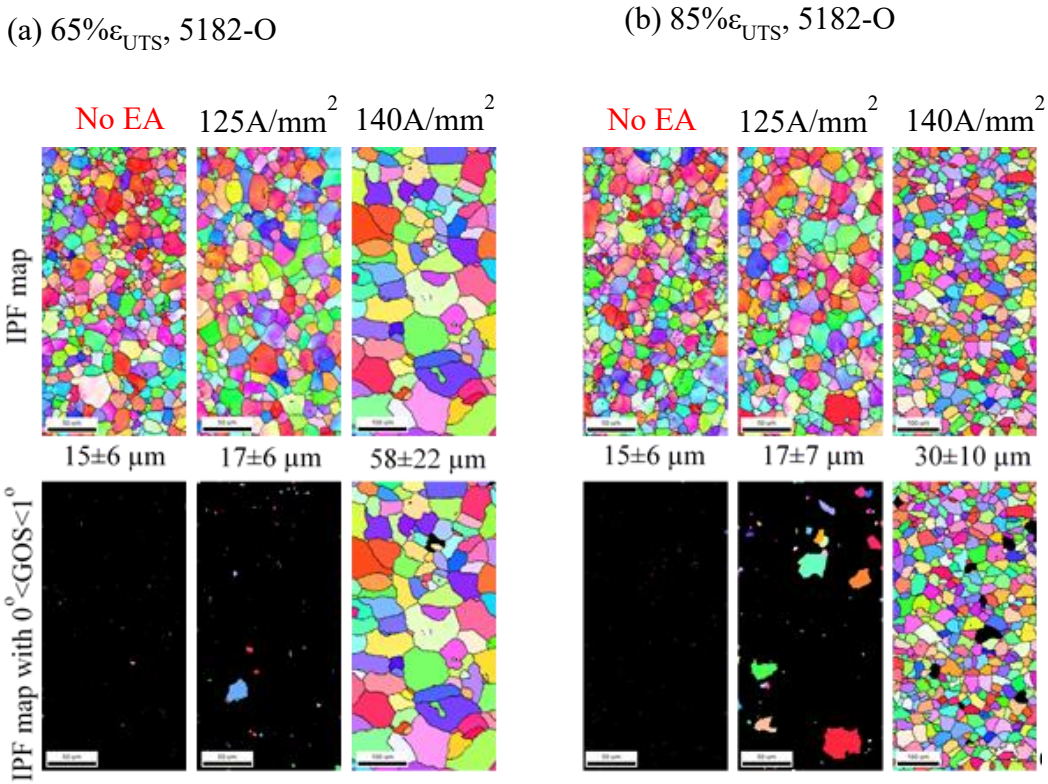

Figure 3.13 The inverse pole figure maps of EA annealed 5182-O aluminum alloys: (a) 65%ε_{UTS}, and (b) 85%ε_{UTS} pre-strain

For the 6061-T6 aluminum alloy, a fully annealed (recrystallized) grain structure was not clearly observed in both 65%ε_{UTS} and 85%ε_{UTS} pre-strained specimens subjected to EA annealing. With the highest electric current density of 140 A/mm^2, a few fully annealed grains were observed, as shown in Fig. 3.14. This is consistent with the FWHM measurements shown in Figs. 3.11(c) and (d). The IPF maps in Fig. 3.14 therefore do not show specific changes in grain size after EA annealing. These results support the argument that the significantly reduced post-EA yield strength of the EA annealed 6061-T6 specimens was due to the combined effects of both EA annealing and EA solid solution treatment.

For the 6061-T6 alloy, the lower extent of EA annealing, which did not reach the extent of full annealing with recrystallization, and the effect of non-uniform temperature distribution along the gage length during EA annealing may not fully explain the effect of electric current on formability, since the increase in electric current density did not induce additional improvement in post-EA elongation in the pre-strained 6061-T6 specimen (Fig. 3.9(b)). The insignificant improvement of post-EA elongation with increasing electric current density for the pre-strained 6061-T6 aluminum alloy may be due to acceleration of microvoid formation around precipitates when electric current was applied [18]. These microvoids play a critical role in the formation of cracks by weakening the bonding force between precipitate particles and matrix, consequently promoting early fractures in 6061-T6 aluminum alloys during EA dual stage forming.

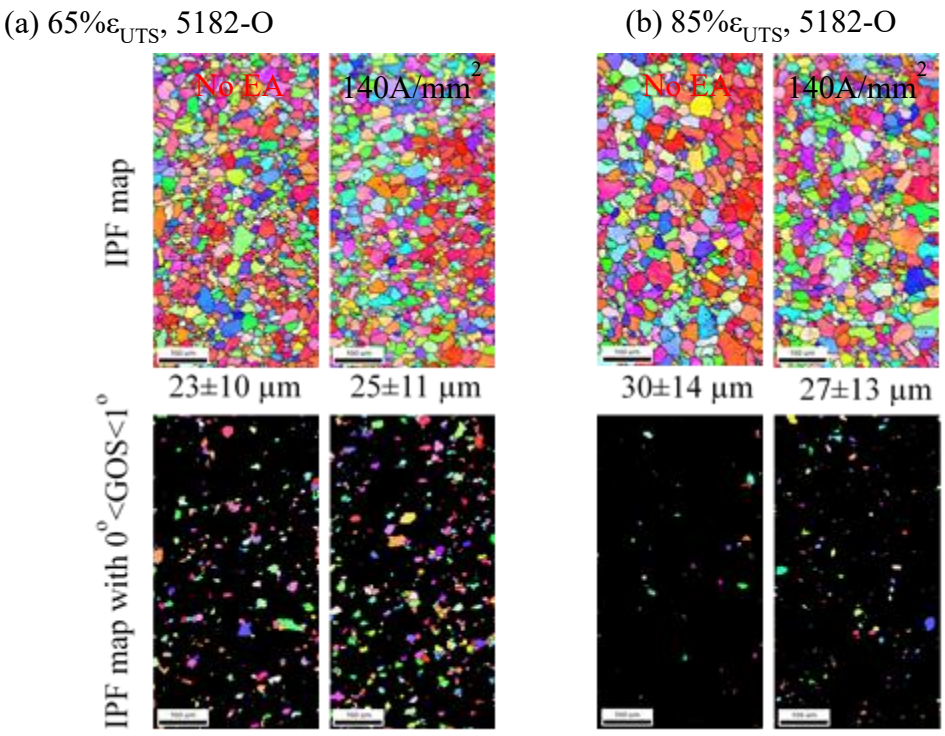

Figure 3.14 The inverse pole figure maps of EA annealed 6061-T6 aluminum alloys: (a) 65% ε_{UTS}, and (b) 85% ε_{UTS} pre-strain

3.7 Summary

The effects of electric current with subsecond duration on the mechanical behaviors and microstructures of two different aluminum alloys were investigated to confirm the concept of dual stage forming with rapid EA annealing. Experimental results clearly demonstrated that subsecond rapid EA annealing by electric current can effectively modify the mechanical behavior of aluminum alloys during stage II of dual stage forming. However, the results also suggest that the effect of electric current on mechanical behavior and microstructure can vary significantly depending on not only electric current parameters but also deformation history (i.e., the amount of preforming in dual stage forming) and the chemical composition of the selected aluminum alloy, as summarized in Table 3.3. In particular, the beneficial effect of EA annealing on formability was limited for the precipitation hardening Al-Mg-Si aluminum alloy selected in the present study relative to the non-heat treatable Al-Mg aluminum alloy. Therefore, while the concept of rapid EA annealing has the potential to improve the productivity of dual stage forming of aluminum alloys, the chemical composition of the target aluminum alloy should be carefully considered in the design of forming process utilizing the concept of rapid EA annealing.

Table 3. A summary of electric current effects

Properties	Condition	5182-O		6061-T6	
		65%ε_{UTS}	85%ε_{UTS}	65%ε_{UTS}	85%ε_{UTS}
Post-EA yield strength	By electric current	Decrease	Decrease	Decrease	Decrease
	Increase of current density	Linear decrease	Linear decrease	Non-linear decrease	Non-linear decrease
Post-EA elongation	By electric current	Increase	Increase	Increase	Increase
	Increase of current density	Increase	Increase	Nearly invariable	Nearly invariable
Total achievable elongation	By electric current	Significant increase	Significant increase	Increase	Increase
	Increase of current density	Increase	Increase	Nearly invariable	Nearly invariable
Dislocation density	By electric current	Decrease	Decrease	Decrease	Decrease
	Increase of current density	Further decrease	Further decrease	Further decrease	Further decrease
Microstruct-ures	At the electric current density of 140 A/mm^2	Recrystallization followed by grain growth	Recrystallization followed by grain growth	Partial recrystallization with some extent of solid solutioning	Partial recrystallization with some extent of solid solutioning

3.8 References for chapter 3

[1] Cole GS, Sherman AM. Lightweight aluminum alloy for automotive application. Material Characterization. 1995; 35:3-9.

[2] Miller WS, Zhuang L. J. Bottem a, AJ Wittebrood, P. De Smet, A. Haszler, A. Vieregge. Mater. Sci. and Eng. A. 2000; 280:37-49.

[3] Dursun T, Soutis C. Recent developments in advanced aircraft aluminium alloys. Materials & Design (1980-2015). 2014 Apr 1; 56:862-71.

[4] Campbell FC, editor. Elements of metallurgy and engineering alloys. ASM International; 2008.

[5] Krajewski PE, inventor; Motors Liquidation Co, assignee. Method for production of stamped sheet metal panels. United States patent US 7,260,972. 2007 Aug 28.

[6] Li J, Carsley JE, Stoughton TB, Hector Jr LG, Hu SJ. Forming limit analysis for two-stage forming of 5182-O aluminum sheet with intermediate annealing. International Journal of Plasticity. 2013 Jun 1; 45:21-43.

[7] Wang K, Li J, Stoughton TB, Carsley JE, Carlson BE. Effect of preform annealing on plastic anisotropy of an age-hardenable Al-Mg-Si alloy. Journal of Materials Processing Technology. 2018 Feb 1; 252:381-8.

[8] Li J, Kim S, Lee TM, Krajewski PE, Wang H, Hu SJ. The effect of prestrain and subsequent annealing on the mechanical behavior of AA5182-O. Materials Science and Engineering: A. 2011 Apr 25;528(10-11):3905-14.

[9] Wang K, He B, Carsley JE, Raghavan RS, Li J, Hartfield-Wünsch SE, Zhang L. Structure–property characterization of an age hardenable Al–Mg–Si alloy after straining and flash annealing. Materials Science and Engineering: A. 2014 Feb 10; 595:25-33.

[10] Fang XW, Xiao H, Marthinsen K, Belyakov A, Fang XY, Huang K. Tailoring microstructure and texture of annealed Al-Mn alloy through the variation of homogenization and prior cold deformation strain. Materials Characterization. 2020 Jun 6:110438.

[11] Harris P. Electromechanical effects in metals. Physical Review B. 1972 Mar 15;5(6):2107.

[12] Roh JH, Seo JJ, Hong ST, Kim MJ, Han HN, Roth JT. The mechanical behavior of 5052-H32 aluminum alloys under a pulsed electric current. International Journal of Plasticity. 2014 Jul 1; 58:84-99.

[13] Kim SJ, Kim SD, Yoo D, Lee J, Rhyim Y, Kim D. Evaluation of the athermal effect of electric pulsing on the recovery behavior of magnesium alloy. Metallurgical and Materials Transactions A. 2016 Dec 1;47(12):6368-73.

[14] Nguyen-Tran HD, Oh HS, Hong ST, Han HN, Cao J, Ahn SH, Chun DM. A review of electrically-assisted manufacturing. International Journal of Precision Engineering and Manufacturing-Green Technology. 2015 Oct 1;2(4):365-76.

[15] Jeong HJ, Kim MJ, Choi SJ, Park JW, Choi H, Luu VT, Hong ST, Han HN. Microstructure reset-based self-healing method using sub-second electric pulsing for metallic materials. Applied Materials Today. 2020 Sep 1; 20:100755.

[16] Li YF, Hong ST, Choi H, Han HN. Solid-state dissimilar joining of stainless steel 316L and Inconel 718 alloys by electrically assisted pressure joining. Materials Characterization. 2019 Aug 1; 154:161-8.

[17] Kim MJ, Lee K, Oh KH. In-Suk Choi, Hyeong-Ho Yu, Sung-Tae Hong, and Heung Nam Han. Electric current-induced annealing during uniaxial tension of aluminum alloy. Scripta Materialia. 2014;75(0):58-61.

[18] Kim MJ, Lee MG, Hariharan K, Hong ST, Choi IS, Kim D, Oh KH, Han HN. Electric current–assisted deformation behavior of Al-Mg-Si alloy under uniaxial tension. International Journal of Plasticity. 2017 Jul 1; 94:148-70.

[19] Fan R, Magargee J, Hu P, Cao J. Influence of grain size and grain boundaries on the thermal and mechanical behavior of 70/30 brass under electrically-assisted deformation. Materials Science and Engineering: A. 2013 Jul 1; 574:218-25.

[20] ASTM E. Standard test methods for tension testing of metallic materials, Annual book of ASTM standards. ASTM.

[21] Engler O, Schäfer C, Myhr OR. Effect of natural ageing and pre-straining on strength and anisotropy in aluminium alloy AA 6016. Materials Science and Engineering: A. 2015 Jul 15; 639:65-74.

[22] Stribeck N. X-ray scattering of soft matter. Springer Science & Business Media; 2007 May 16.

[23] Li J, Carsley JE, Stoughton TB, Hector Jr LG, Hu SJ. Forming limit analysis for two-stage forming of 5182-O aluminum sheet with intermediate annealing. International Journal of Plasticity. 2013 Jun 1; 45:21-43.

[24] Park JW, Jeong HJ, Jin SW, Kim MJ, Lee K, Kim JJ, Hong ST, Han HN. Effect of electric current on recrystallization kinetics in interstitial free steel and AZ31 magnesium alloy. Materials Characterization. 2017 Nov 1; 133:70-6.

[25] Luu VT, Dinh TK, Das H, Kim JR, Hong ST, Sung HM, Han HN. Diffusion Enhancement during Electrically Assisted Brazing of Ferritic Stainless Steel Alloys. International Journal of Precision Engineering and Manufacturing-Green Technology. 2018 Oct 1;5(5):613-21.

[26] Humphreys FJ, Hatherly M. Recrystallization and related annealing phenomena. Elsevier; 2012 Dec 2.

Chapter 4

Conclusion

Electrically assisted (EA) rapid heat treatment is a promising alternative heat treatment method, in which the microstructure and mechanical properties of a metal alloy are modified by simply applying pulsed electric current for a short duration in sheet metal forming process. The reduced flow stress and increased ductility, which are often called the electroplastic effect, are generally observed in electrically assisted forming process. Many scholars have been proposed to explain the effectiveness of the electric current to formability of metals during forming process. In certain instances, the mechanical behavior of metals when applying electric current could be nicely described based on the thermal effect which caused by resistive Joule heating. However, from the report of many other studies, the well-known resistive Joule heating is not enough to clearly clarify this phenomenon without considering the athermal electroplastic factor of the electron wind effect.

Recently, the combination of the athermal effect of electricity and the thermal effect of rapid resistance heating is widely employed to explain the effectiveness of EA rapid heat treatment during forming.

Even though the performance of EA rapid heat treatment in sheet metal forming process surpasses that of conventional heat treating, the mechanism of electricity

effect is not identified. Also, the quantitative effect of electric current on the microstructure and resultant mechanical behavior is not evaluated yet.

The objective of present study is mainly consisted of two parts. Firstly, the intermetallic evolution of Al-Si coated hot stamping steel during EA rapid heating is experimentally investigated based on the microstructure analysis. Also, a modified EA rapid heating of Al-Si coated hot stamping steel is suggested. Based on the understanding of electric current assisted phenomenon, finally, the effect of EA annealing on the mechanical behaviors of two different pre-strained aluminum alloys is reported.

Firstly, Al-Si coating on hot stamping steel normally transfers to brittle intermetallic phase which induces poor mechanical properties to the steel substrate. Thus, the modified EA rapid heating of Al-Si coated hot stamping steel was suggested in chapter 2 in order to improve the intermetallic evolution during the heating process. In the modified EA rapid heating, a continuous electric current for a suitable duration is applied to a specimen to heat it to a temperature slightly below the melting temperature of the coating. The temperature of the specimen is then kept constant for specified dwell time. The result of the microstructural analysis shows that the modified EA rapid heating could effectively increase the thickness of the intermetallic layer between the coating and steel substrate much faster than conventional furnace heating and induction heating. The effectiveness of EA rapid

heating may be due to the athermal effect of the electric current on the mobility of atoms, in addition to the well-known resistance heating effect. EA rapid heating also provides a technical advantage in that partial austenization can be easily achieved by properly placing the electrodes, as demonstrated in the present study.

Secondly, through the understanding of the mechanism of electricity effect during EA rapid heating, the effect of EA annealing on the mechanical behaviors of pre-strained two different aluminum alloys during EA dual-stage forming are experimentally investigated in chapter 3. At first, a specimen is deformed to a specific pre-strain by uniaxial tension and then automatically unloaded. After that, the pre-strained specimen is subjected to electrically assisted annealing by electric current with a fixed subsecond duration. Finally, the specimen is reloaded until fracture. Experimental results show that application of electric current with a subsecond duration induces electrically assisted annealing to both pre-strained aluminum alloys. The electric current also increases total achievable elongation until fracture during electrically assisted dual stage forming for both aluminum alloys. However, analysis of the stress-strain behavior during reloading and microstructural observations suggest that the quantitative effects of electric current on the post-electrically assisted annealing mechanical behavior and resultant microstructure are strongly dependent on the type of aluminum alloy. With the electric current density of 140 A/mm^2, a full recrystallization followed by grain growth occurs in the pre-strained Al-Mg alloy specimens. For the pre-strained Al-

Mg-Si alloy specimens, the electric current density of 140 A/mm^2 induces both annealing and solid solutioning. Together, our findings indicate that while electrically assisted annealing is effective at improving the productivity of dual stage forming of an aluminum alloy, the composition of the aluminum alloy should be carefully considered in the design of forming process utilizing the concept of electrically assisted annealing since the beneficial effect was limited for the precipitation hardening 6061-T6 aluminum alloy.

From this study, the concept of EA rapid heat treatment in sheet metal forming is suggested. Also, the intermetallic evolution of Al-Si coated hot stamping steel, and the mechanical behavior of pre-strained two different aluminum alloys during EA rapid heating is investigated clearly. The optimal condition to achieve the efficiency of the process is accomplished considering both microstructure and mechanical behavior aspects. Through the athermal effect of electric current on the mobility of atoms, in addition to the well-known resistance heating effect, EA rapid heating is a feasible technique to apply in the real industry with the significant benefits in process cycle time reduction.